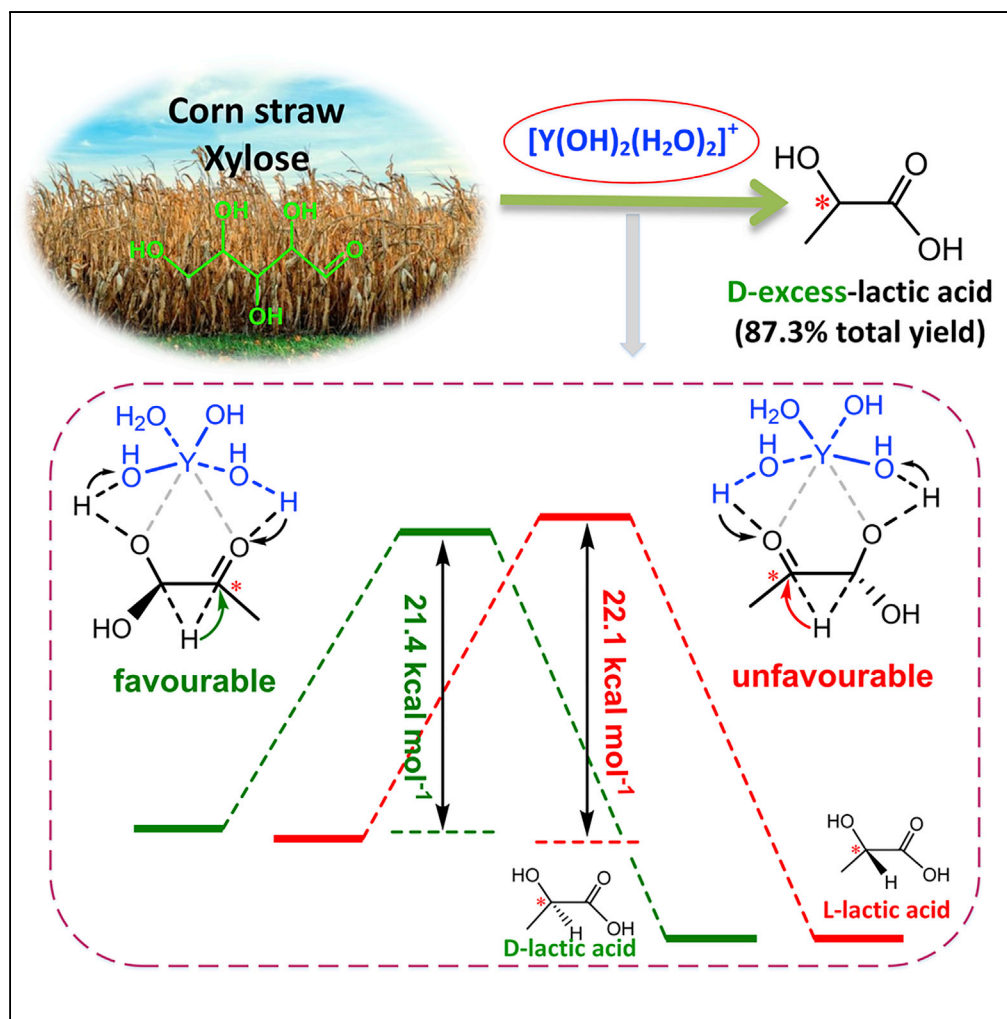**Article**

D-Excess-LaA Production Directly from Biomass by Trivalent Yttrium Species

Shuguang Xu, Jing Li, Jianmei Li, Yi Wu, Yuan Xiao, Changwei Hu

lijianmei@scu.edu.cn (J.L.)
changweihu@scu.edu.cn (C.H.)

HIGHLIGHTS

Y(III) exhibited outstanding efficiency for biomass conversion to lactic acid

A high yield of D-excess-lactic acid with 20% ee value was obtained from xylose

Reaction mechanism was successfully revealed by isotopic labeling and DFT study

The lower strain energy induced the enantioselective formation of D-lactic acid

Article

D-Excess-LaA Production Directly from Biomass by Trivalent Yttrium Species

Shuguang Xu,[1] Jing Li,[1] Jianmei Li,[1,*] Yi Wu,[1] Yuan Xiao,[1] and Changwei Hu[1,2,*]

SUMMARY

D-lactic acid (D-LaA) synthesis directly from actual biomass via chemocatalytic conversion has shown high potential for satisfying its enormous demand in widespread applications. Here we report yttrium (Y(III))-species-catalyzed conversion of xylose and raw lignocelluloses to LaA with the highest yield of 87.3% (20% ee to D-LaA, ee%=(moles of D-LaA - moles of L-LaA)/(moles of D-LaA + moles of L-LaA) × 100). Combining experiments with theoretical modeling, we reveal that $[Y(OH)_2(H_2O)_2]^+$ is the possible catalytically active species, enabling the unconventional cleavage of C3-C4 in xylulose and the subsequent dehydration of glyceraldehyde to pyruvaldehyde (PRA). The distinct interactions between hydrated-PRA and $[Y(OH)_2(H_2O)_2]^+$ species contribute to the formation of different enantiomers, wherein H-migration via *re*-face attack leads to L-LaA and that via *si*-face attack yields D-LaA. The lower strain energy barrier is the origin of excess D-enantiomer formation.

INTRODUCTION

Valuable chemical production directly from renewable lignocellulosic biomass is of great importance in seeking a sustainable future and bio-based economy, whereas chiral chemical production is still challenging owing to the quite complicated structure of biomass (Zhang et al., 2017; Liu et al., 2017; Farrán et al., 2015; Ennaert et al., 2016). Lactic acid (LaA), as one of the top 15 platform chemicals derived from carbohydrates, has been widely used in food and pharmaceuticals, especially in the production of polylactic acid (PLA), which has shown high potential in medical and clinical applications owing to its excellent biodegradability and biocompatibility (Castillo Martinez et al., 2013; Delidovich et al., 2016). The property of PLA is greatly dependent on the ratio of D-/L-LaA. Particularly, when poly D-LaA is blended with poly L-LaA to form a stereocomplex structure, it has been pointed out that the thermal stability, mechanical performance, and hydrolysis resistance can be significantly improved (Davachi and Kaffashi, 2015; Chen et al., 2016; Nagarajan et al., 2016; Lasprilla et al., 2012). The booming of PLA industry greatly stimulates the development of LaA production (Dusselier et al., 2013). However, there is a huge gap between the production capacity and actual output of LaA, and bulk commercial supply of LaA with an excess of D-enantiomer is still unavailable (Dusselier et al., 2013).

Currently, over 90% of commercial LaA is produced by fermentation of carbohydrates with mainly L-LaA in excess, whereas it is still hard to produce D-LaA with the same productivities and purities (Baek et al., 2016; Eş et al., 2018). The high cost of enzymes and waste disposal in fermentation, in addition to the restricted feedstock, including only hexose sugars and edible di-/polysaccharides, greatly inhibit its widespread application (Desguin et al., 2014; Abdel-Rahman et al., 2013; Maki-Arvela et al., 2014). Novel chemocatalytic methods using homogeneous (Li et al., 2017; Sharninghausen et al., 2014) or heterogeneous (Coman et al., 2015; Holm and Taarning, 2010; Besson et al., 2014) catalysts for LaA production therefore have attracted increasing attention in recent years, owing to the high production capacity, widened starting resources even including non-edible cellulose and actual biomass (Wang et al., 2013; Deng et al., 2018; Dusselier and Sels, 2014; Lin et al., 2013; Gallezot, 2012; Tuck et al., 2012; Dapsens and Mondelli, 2015), easily available catalysts, as well as the avoided formation of waste salts. However, the recent advances are mainly focused on the use of non-edible cellulose. To enhance LaA productivity and meet the rapid increase of LaA demand, it is essential to take full advantages of all carbohydrates in biomass, including not only hexose but also pentose (Mäkiarvela et al., 2011). Nevertheless, pentose-based feedstock is rarely employed for LaA production. Even in the limited reports, the yield of LaA (<45%) is unsatisfactory, because the catalyst is usually not as effective as that for hexose conversion (Yang et al., 2015, 2016a, 2016b). Moreover, it is regrettable that the production of chiral LaA directly from actual biomass via chemocatalysis cannot be found in all the references we can find. In the existing reports, there is little information on the distribution of LaA enantiomers via chemocatalysis especially when pentose- and hexose-based

Reactant	Xylose	Xylose	Xylose	Xylose	Xylose	Xylan	M-Cellulose	Corn Straw
Catalyst	Y(III)	Cr(III)	Al(III)	Pb(II)	Sn(II)	Y(III)	Y(III)	Y(III)
Yield (%)	87.3	26.6	34.2	41.7	45.0	72.5	57.0	61.8
ee value (%)	20	17	17	23	26	16	12	12
Carbon balance (%)	70	63	61	65	65	71	67	65

Table 1. The Catalytic Performance of Metal Ions on the Conversion of Xylose and Biomass to LaA[a]

[a]Reaction conditions: 0.20 g xylose (26.7 mM) or 0.20 g M-cellulose or 1.0 g corn straw; 50 mL H_2O; 6.6 mM YCl_3; N_2, 2 MPa; temperature, 493 K; reaction time, 0.5 h. The high-performance liquid chromatography analysis results of the mixture of D/L-lactic acid is shown in Figure S1.

carbohydrates are used as feedstock. Here, we achieve the production of D-excess-LaA with outstanding yield using a simple achiral yttrium (Y(III)) ion directly from pentose-based feedstock and actual biomass, that is, corn straw, eliminating the need of complex chiral catalyst in conventional asymmetric synthesis (Otocka et al., 2017; Feng et al., 2017) and the extraction of monosaccharide from raw biomass. We use ^{13}C-C1-labeled xylose and D_2O as probe molecules to gain deep insights into the active species and reaction mechanism, by combining experiments with quantum chemical modeling. Significantly, we have also proposed the origin of D-/L-enantiomer formation and explained the reason why more D-LaA is produced with the assistance of (Y(III)) ion, for the first time.

RESULTS AND DISCUSSION

Catalytic Activity of Y(III)

We first investigated the catalytic activity of Y(III) for xylose conversion to LaA (Figure S2). We found that Y(III) greatly enhanced xylose conversion, giving as high as 87.3% yield of LaA with 20% ee value to D-LaA, ee% =(moles of D-LaA - moles of L-LaA)/(moles of D-LaA + moles of L-LaA) ✕ 100 at 493 K for 0.5 h with limited by-products (Figure S3), whereas only limited LaA (3.2%) with a D-/L-LaA ratio of ∼1:1 was obtained for the blank reaction. We also investigated the catalytic efficiency of other metal ions, including Cr(III), Al(III), Pb(II), and Sn(II) (Table 1). Similarly, more D-LaA than L-LaA was obtained. This is different from the fermentation route wherein more L-LaA is usually obtained (Abdel-Rahman et al., 2013). Although Pb(II) and Sn(II) had been proved to show high efficiency for hexose conversion to LaA in the literature (Wang et al., 2013; Deng et al., 2018), they failed to effectively promote xylose conversion to LaA in this study with yields of only 41.7% and 45.0%, respectively. Y(III) outperformed other selected metal ions, achieving the highest LaA yield among these selected metal ions and those used in the literature (Table S1). To extend the application of the Y(III) system, we further employed xylan, microcrystalline cellulose (M-cellulose), and corn straw as feedstock. Yields of LaA were 72.5% (16% ee) and 57.0% (12% ee) from xylan (Figure S4) and M-cellulose, respectively, whereas 61.8% (12% ee) yield was obtained based on the amounts of cellulose and hemicellulose from corn straw (Table 1). This indicates that Y(III) exhibits multiple catalytic performances, integrating the depolymerization of hemicellulose and cellulose with the next monosaccharide conversion to yield LaA. Furthermore, we performed the separation and recycling of Y(III) ion from reaction solution by a chemical precipitation method (Note S1 and Figure S5) and found that the recycled Y(III) showed almost the same catalytic activity within three runs (Table S2).

Determination of Active Species

Considering the high efficiency of Y(III), we conducted several control experiments with HCl as catalyst and xylose as feedstock to identify the active catalytic species in Y(III) system. With similar pH value (pH = 5.5) to YCl_3 aqueous solution, HCl showed little activity for LaA formation (total yield ≤ 1.4%) but sharply increased furfural (FF) yield (Figure S6B), accompanied by a low carbon balance (Figure S7). Similarly, by the addition of equivalent HCl to the Y(III) system, LaA yield sharply declined from 87.3% to 57.1%, and continuously increasing the HCl amount to 120 mM gave only 3.6% yield of LaA (Figure S8, Table S3). We therefore consider that Y(III) predominantly contributes to the effective promotion of LaA yield, whereas the functions of both H^+ generated from YCl_3 hydrolysis and Cl^- are relatively weak. We also conducted a series of experiments with Y(III) in neutral and alkaline media (Figure S9). It was found that the yield of LaA sharply decreased by increasing the pH value from 5.5 to 10.5, and only 10.7% yield of LaA was obtained at pH = 10.5, possibly attributed to the formation of $Y(OH)_3$ precipitate. Therefore, the highest LaA yield was achieved at pH = 5.5 when Y(III) was autohydrolyzed in neutral aqueous solution. ESI-MS (electrospray ionization mass spectrometry) analysis of YCl_3 aqueous solution exhibited obvious

peaks of hydrolyzed Y(III) species $[Y(OH)_2(H_2O)_n]^+$ (n = 0, 2, 4) (Figure S10A). Further introduction of xylose (Figure S11) to YCl_3 aqueous solution also gave $[Y(OH)_2(H_2O)_n]^+$ intermediates, which combined with other chemicals such as xylose and FF (Figures S10B and S12), and ESI-tandem MS analysis gave obvious fragment peaks of $[Y(OH)_2(H_2O)_n]^+$ (Figure S13). Theoretical computation also demonstrated that the formation of these intermediates was feasible under the reaction conditions (Figure S10G). HCl addition could suppress the hydrolysis of Y(III), which was proved by the gradually disappearing peak of $[Y(OH)_2(H_2O)_n]^+$ by ESI-MS analysis with increasing HCl amount (Figure S14). All these results suggest the important function of $[Y(OH)_2(H_2O)_n]^+$ species for xylose conversion. The results of theoretical computation indicated that the stabilization energy of Y(III) hydrolyzing to $[Y(OH)_2(H_2O)_2]^+$ (26.9 kcal mol^{-1}, Note S2) was the highest among these species $[Y(OH)_2(H_2O)_n]^+$ (n = 0–4) (Figure S15). It is therefore plausible to assume that $[Y(OH)_2(H_2O)_2]^+$ is the active species in xylose conversion to LaA.

The Performance of Active Species on Xylose Conversion to PRA

We then attempted to reveal the performances of active species on LaA formation from xylose. In the process of xylose conversion to LaA with the assistance of Y(III), we observed the successive formation of xylulose and triose (dihydroxyacetone [DHA], glyceraldehyde [GLA], and pyruvaldehyde [PRA]) intermediates. We therefore speculate that LaA formation may pass through xylose isomerization to xylulose and the consequent C-C cleavage to trioses. It is reported that the bottleneck in LaA production from pentose is the selective splitting of C-C bond, and two distinct C-C cleavage mechanisms have been proposed in the literature (Yang et al., 2015; Holm et al., 2012). One involves C2-C3 cleavage in aldopentose via a retro-aldol condensation reaction yielding GLA and glycolaldehyde. This is a widely accepted pathway. The other involves C3-C4 cleavage in ketopentose via a retro-aldol condensation giving DHA and glycolaldehyde. To reveal the performance of $[Y(OH)_2(H_2O)_2]^+$ on C-C cleavage in xylose, we employed ^{13}C-C1-labeled xylose as substrate and D_2O as solvent. In the presence of Y(III), almost all labeled ^{13}C was transferred into the methyl carbon atom of LaA after reaction (Figures 1C and S16), whereas no ^{13}C was found in glycolic acid (Figure S17). Without catalyst, several by-products with labeled ^{13}C such as formic acid (Figure S18) and FF (Figure S19) were detected after reaction (Figure 1B), whereas no ^{13}C-labeled LaA was observed. This demonstrates that $[Y(OH)_2(H_2O)_2]^+$ can facilitate C3-C4 cleavage in xylose under the reaction conditions in this work (Figure 2, Scheme S1), which is different from the result in the literature wherein C2-C3 cleavage predominantly contributes to LaA formation from xylose (Yang et al., 2015, 2016a, 2016b).

Given the cleavage of C3-C4 in xylulose, the resulting DHA can be transformed to GLA in water by means of keto-enol tautomerization. To further reveal the performance of $[Y(OH)_2(H_2O)_2]^+$ on triose conversion to LaA, we conducted control experiments using trioses (DHA, GLA, PRA) as substrates. We found that Y(III) addition greatly enhanced the conversion of these trioses to LaA with much higher yield (≥92%, Figure S20 and Table S4) compared with that without catalyst (≤12%). We then used D_2O as solvent in place of H_2O (Figures S21 and S22 and Table S5) and observed the formation of LaA with deuterated methyl group when DHA and GLA were used as substrates (Figure S21, Table S5 entries 5 and 6), in agreement with the result of Sels et al. (Pescarmona et al., 2010). Similarly, LaA with deuterated methyl was obtained from xylose conversion under the same conditions (Figure S23, Table S5 entry 2). Nevertheless, no LaA with deuterated methyl was detected to be derived from DHA and GLA without Y(III) (Table S5 entries 8 and 9). Just heat treatment of LaA-D_2O solution with/without Y(III) (Table S5 entries 3 and 4) cannot induce the formation of LaA with deuterated methyl group. These results suggest that DHA/GLA undergoes a dehydration reaction to form PRA with the assistance of Y(III). A detailed time course analysis showed that LaA yield sharply increased once PRA began to decrease in the presence of Y(III) (Figure S24). In combination with the fact that PRA exhibits the highest conversion rate to LaA among these three trioses, we infer that PRA is the most advantageous triose for LaA formation. However, in the case of PRA as substrate with Y(III) as catalyst, no LaA with deuterated methyl group was observed (Figure S21C, Table S5 entry 7), implying the H-migration from C1 to C2 in PRA before LaA formation. In addition, no D atom was connected with C2 of LaA in all cases, implying that the H atom in C2 of LaA originated from the aldehyde group. This further confirms H-migration from C1 to C2 (Scheme S2). Combining with the above-mentioned experimental results, we tentatively propose that LaA formation from xylose with the aid of Y(III) may proceed through the following pathways (Figure 3A): (1) xylose isomerization to xylulose; (2) C3-C4 cleavage of xylulose to DHA and DHA isomerization to GLA, along with a side reaction involving xylose dehydration to FF; (3) DHA/GLA dehydration to PRA via ketone-aldehyde tautomerism; and (4) PRA hydration and H-migration from C1 to C2, finally leading to LaA.
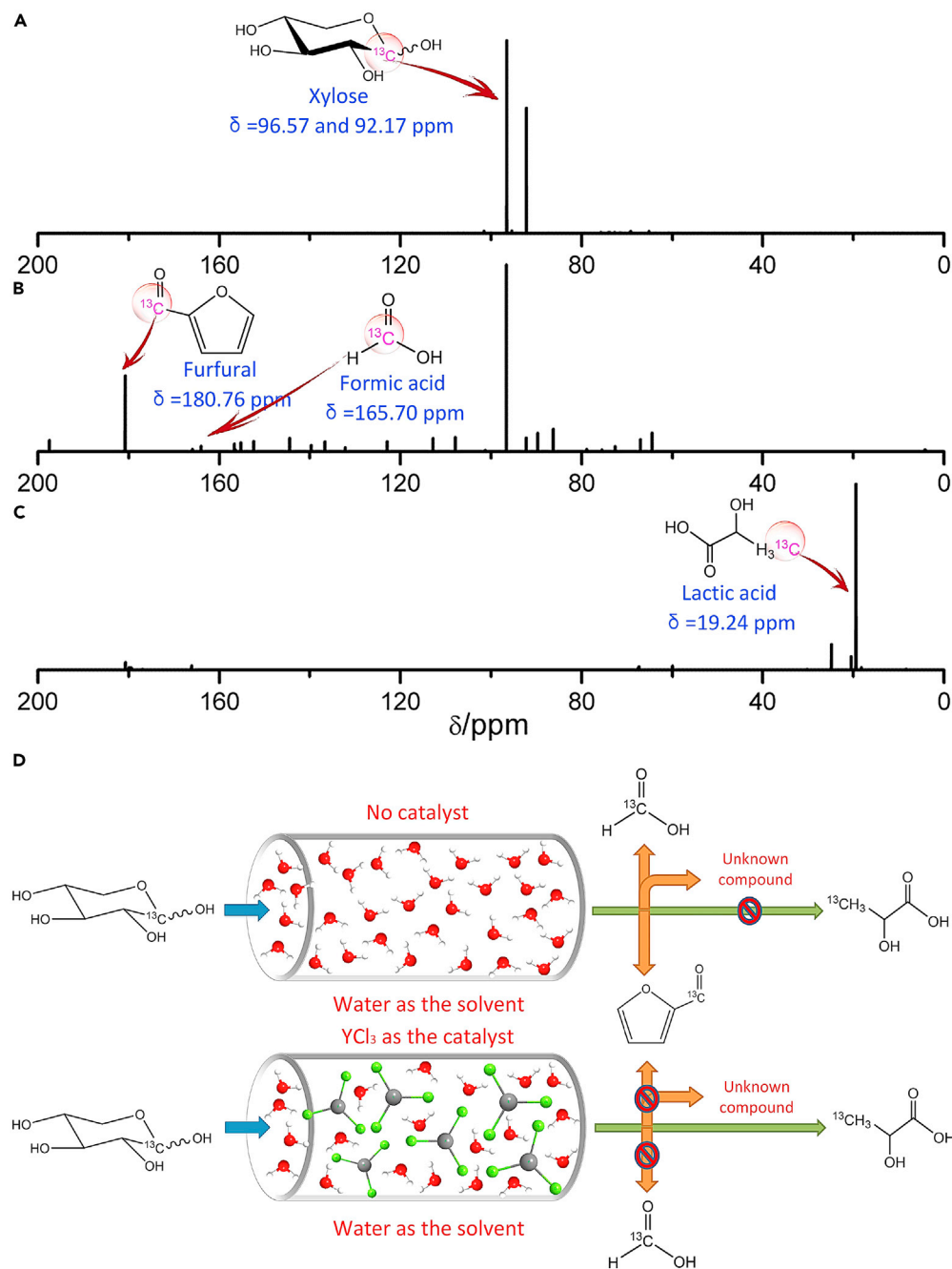
Figure 1. ^{13}C NMR Spectra of Different Mixture and the Schematic Diagram for the flow of ^{13}C Labeled Atoms from ^{13}C1-xylose with/without Y(III)

(A–D) ^{13}C NMR spectra of (A) mixture of ^{13}C1-xylose with D_2O at room temperature, (B) liquid products of ^{13}C1-xylose conversion in D_2O without catalyst, and (C) liquid products of ^{13}C1-xylose conversion with Y(III). (D) Schematic diagram for the flow of ^{13}C-labeled atoms with/without Y(III). Reaction conditions: 0.20 g (26.7 mM) ^{13}C1-xylose; 50 mL D_2O; 6.6 mM YCl_3 (if catalyst was used); N_2, 2 MPa; 0.5 h; 493 K.

We next conducted quantum chemical computation, aiming at getting more insights into the reaction mechanism at the molecular level, as well as explaining how $[Y(OH)_2(H_2O)_2]^+$ species have a decisive influence on the catalytic reaction. We found that the results of quantum chemical computation were consistent with those in experiments. The addition of $[Y(OH)_2(H_2O)_2]^+$ significantly reduced the activation barrier of xylose isomerization to xylulose from 32.9 (non-catalytic reaction) to 17.4 kcal mol^{-1} (Table S6).
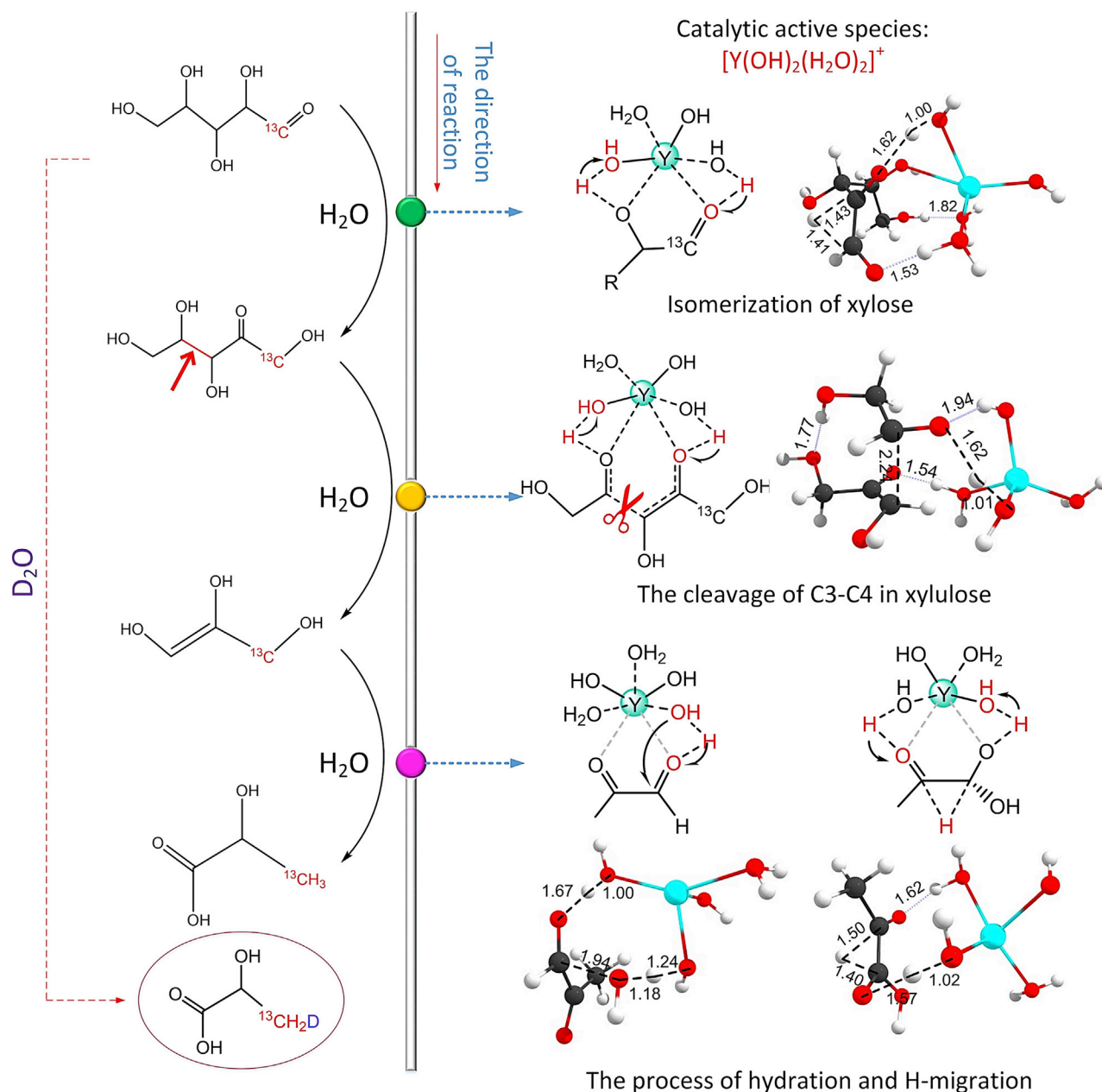
Figure 2. Scheme of ¹³C1-Xylose Conversion to ¹³C-LaA with Y(III)
Bond lengths are reported in angstroms.

We attribute it to a different H-migration from C2-O to C1-O of xylose aided by a water molecule between $[Y(OH)_2(H_2O)_2]^+$ and xylose (Figure S26), which is more effective than the conventional direct proton transfer in references (Yang et al., 2016a, 2016b; Román-Leshkov et al., 2010). Subsequently, $[Y(OH)_2(H_2O)_2]^+$ species continued to induce and accelerate C3-C4 cleavage of xylulose with an 18.8 kcal mol⁻¹ energy barrier, passing through the similar H-shift from C4-OH to C2-O helped by a water molecule (Figure S27). 1-Ene-propanetriol (4 in Figure 3, captured in ESI-MS spectra [Figure S28]) was generated after C3-C4 cleavage, which was easily converted to DHA with an 11.3 kcal mol⁻¹ energy barrier. The remaining C2 compound was transformed to glycolic aldehyde. The energy barrier for the next aldehyde-ketone isomerization of DHA to GLA also decreased from 32.6 (non-catalytic pathway) to 19.7 kcal mol⁻¹ (Figure S29). Without catalyst, huge energy barrier ($\Delta G^{\neq}$ = 78.9 kcal mol⁻¹) was required for C3-C4 cleavage (Figure S30), and the direct breaking of C2-C3 in xylose via the conventional retro-aldol
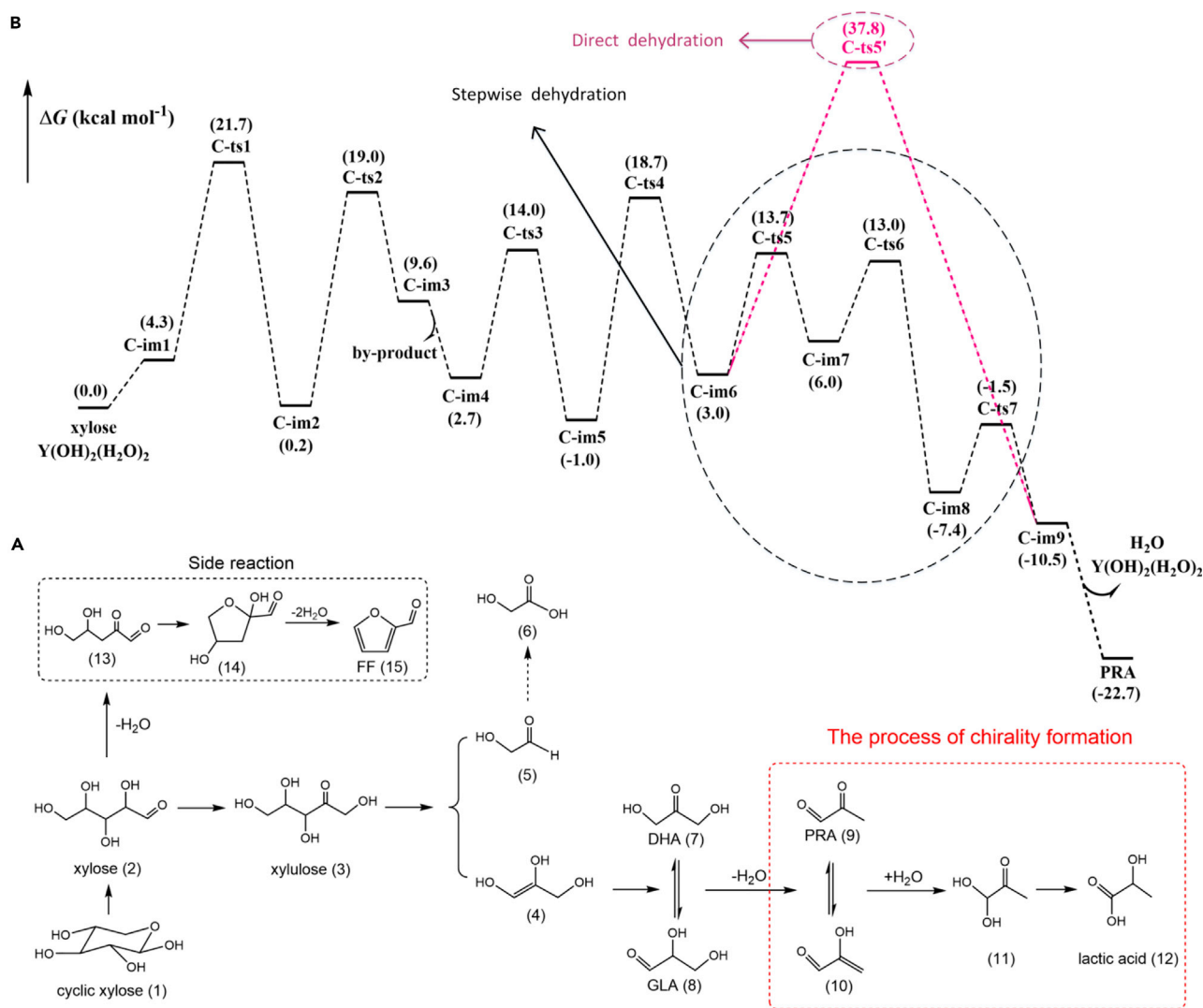
Figure 3. The Proposed Reaction Pathway of Xylose to PRA and the Corresponding Energy Profiles

(A and B) The proposed reaction pathway of xylose conversion to PRA catalyzed by Y(III) species (A) and the corresponding energy profiles (B) (in kcal mol^{-1}, all the mentioned optimized geometries are shown in Figure S25 and the corresponding Cartesian coordinates are showed in Table S8).

condensation also showed a 76.4 kcal mol^{-1} energy barrier (Figure S31). The next GLA dehydration to PRA is widely considered as the rate-limiting step in the process of conversion of trioses to LaA in the literature (Rasrendra et al., 2010), due to the high-energy barrier (59.6 kcal mol^{-1}) without catalyst. In this study, [Y(OH)$_2$(H$_2$O)$_2$]$^+$ significantly promoted GLA dehydration to PRA through three steps: (1) –OH in [Y(OH)$_2$(H$_2$O)$_2$]$^+$ deprived H atom on C2 to form H$_2$O; (2) C3-hydroxyl protonation and H$_2$O leaving, yielding chemical **10**; and (3) isomerization of **10** to PRA. The energy barriers of these three steps were 10.7, 7.0, and 5.9 kcal mol^{-1}, respectively (Figure S32 and Table S7).

The Origin of D-/L-Enantiomer Formation

The following PRA conversion to LaA is commonly considered to be an intra-molecular Cannizzaro reaction, which is easier under alkaline conditions (Yang et al., 2016a, 2016b; Dong et al., 2016). We also obtained LaA from PRA with high yield when replacing Y(III) with equivalent amount of NaOH (Table S9). Our calculations showed that LaA formation from PRA might undergo sequential hydration of aldehyde group and H-migration from C1 to C2 (Figure 4). With the aid of [Y(OH)$_2$(H$_2$O)$_2$]$^+$, PRA hydration showed lower activation energy barrier than that via non-catalytic pathway (Table S6). The next H-migration proceeded via three steps: (1) the H transfer from C1-OH to [Y(OH)$_2$(H$_2$O)$_2$]$^+$; (2) the next H-migration from
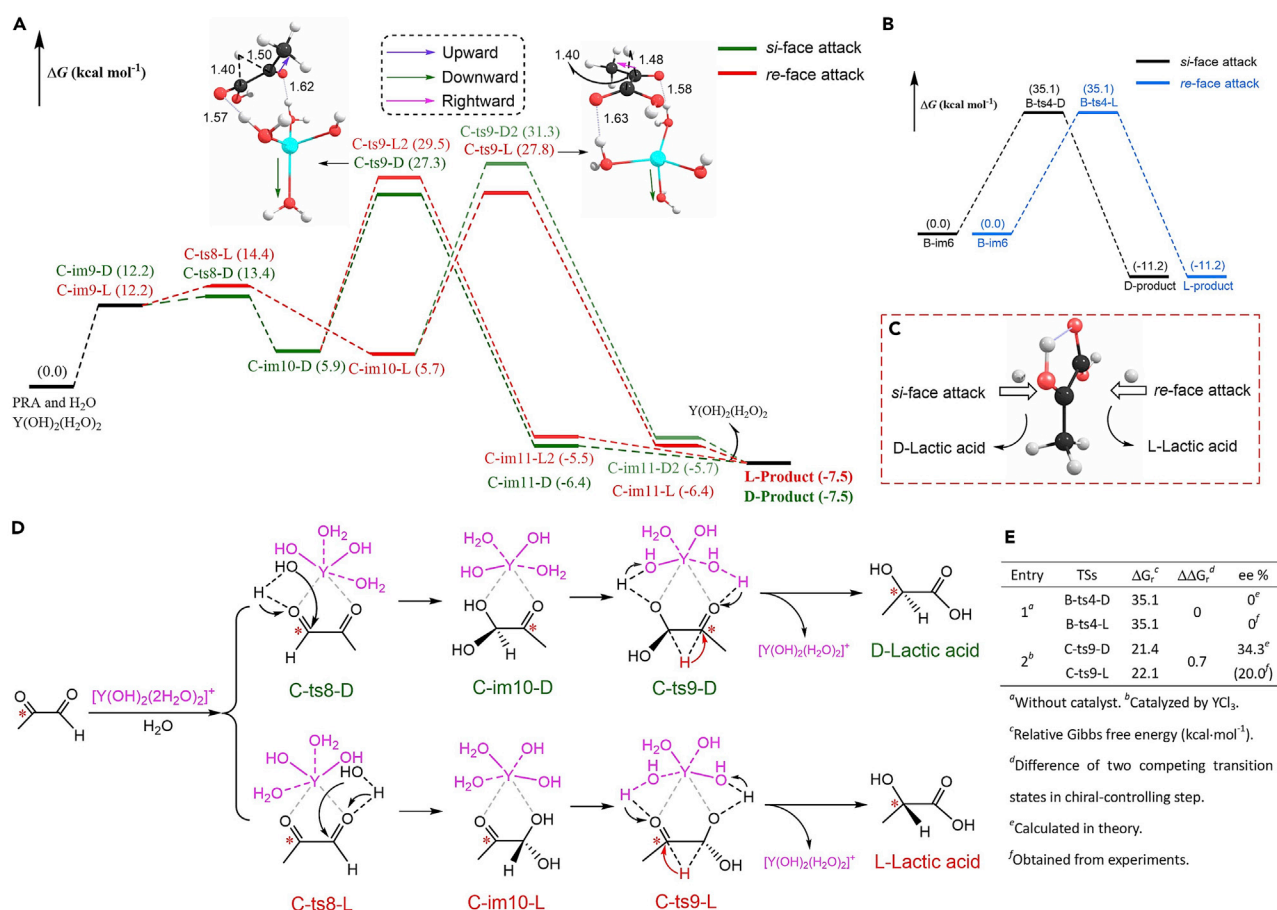
Figure 4. The Proposed Reaction Pathway on the Formation of Lactic Acid Enantiomers from PRA

(A–E) (A) the energy profiles for catalytic pathway; (B) the energy profiles for the key chirality-controlling step in non-catalytic pathway; (C) the graphic for the formation of chiral center in non-catalytic pathway; (D) the proposed reaction pathway for the formation of lactic acid enantiomers from PRA catalyzed by Y(III) species; (E) the relative Gibbs energy (ΔG_r, kcal mol^{-1}) and the corresponding energy difference ($\Delta \Delta G_r$, kcal mol^{-1}) of competing transition in chirality-controlling step between catalytic pathway and non-catalytic pathway and the corresponding stereo-selectivity (ee%) (all the mentioned optimized geometries in Figure 4A are shown in Figure S33 and the corresponding Cartesian coordinates are shown in Table S8). Bond lengths are reported in angstroms.

H$_2$O in [Y(OH)$_2$(H$_2$O)$_2$]$^+$ to C2, that is, water in catalyst assists H transfer; (3) another H from C1 directly to C2 is the crucial step for the formation of different LaA enantiomers. We found that the H-migration from C1 to C2 via *si*-face attack of hydrated PRA could lead to D-LaA, whereas *re*-face attack gave L-LaA (Figure 4C). Without catalyst, the activation energy barrier of D-LaA formation was equal to that of L-LaA formation (35.1 kcal mol^{-1}, Figures 4B and 4E). This is possibly ascribed to the similar steric hindrance of *si*-face attack to that of *re*-face attack, thus giving a racemic mixture. This is well in agreement with the experimental result. By contrast, in the presence of [Y(OH)$_2$(H$_2$O)$_2$]$^+$, hydrated PRA could interact with [Y(OH)$_2$(H$_2$O)$_2$]$^+$ via two different ways, finally yielding two distinct intermediates C-im10-D and C-im10-L, both of which could result in the formation of D- and L-LaA enantiomers via different transition states (Figures 4A and 4D). Time-of-flight (TOF) analysis (Table S10) demonstrates that the TOF value of catalytic cycle to D-LaA via C-ts9-D is much higher than that to L-LaA via C-ts9-L2, and the pathway to L-LaA via C-ts9-L also shows much higher TOF value than that to D-LaA via C-ts9-D2. We then compared these two predominant pathways and found that D-LaA formation via C-ts9-D exhibits much higher TOF value than L-LaA formation via C-ts9-L. However, we found that H-migration in C-ts9-D via *si*-face attack showed similar steric hindrance to that in C-ts9-L via *re*-face attack. To investigate the actual chirality-determining factor, we further conducted activation strain analysis (Table S11) and found that the strain energy barrier for C-ts9-D (97.0 kcal mol^{-1}) was much lower than that of C-ts9-L (107.5 kcal mol^{-1}), which led to lower $\Delta E^{\neq}$ of C-ts9-D than that of C-ts9-L, although the interaction energy of C-ts9-D between catalyst and hydrated

PRA was higher than that of C-ts9-L. Thus, it seems that the reaction cycle via C-ts9-D is more competitive than that via C-ts9-L, with a 0.7 kcal mol^{-1} lower activation energy barrier (Figure 4A). We therefore speculate that the lower strain energy between the catalyst and reactant enables the formation of a little more D-LaA with a calculated ee value of 34.3% (Figure 4E), according to Curtin-Hammett principle (Schneebeli et al., 2009), which is close to the 20% ee value obtained in the experiment. In the process of triose to D-/L-LaA, the final H-migration from C1 to C2 becomes the rate-limiting step, which is also the chirality-controlling step for xylose conversion to D-/L-LaA in this catalytic system.

Conclusions

Y(III) outperforms other selected metal ions, achieving an outstanding LaA yield from xylose and corn straw. $[Y(OH)_2(H_2O)_2]^+$, as the possible active species, primarily contributes to C3-C4 cleavage of xylose, leading to LaA formation via an unconventional pathway. The formation of D-/L-enantiomer is significantly dependent on the different interactions between hydrated PRA and catalytically active species. Water coordinated with Y(III) and the reactant itself construct a chiral environment, and the function of water for helping chiral catalysis might be popular in natural life process. The lower strain energy results in enantioselectivity favoring D-LaA. To the best of our knowledge, this is the first detailed description of the enanotioselectivity of LaA enantiomer obtained from actual raw biomass containing pentose and hexose via chemocatalytic conversion, and also the first attempt to reveal the formation mechanism of LaA enantiomers. Although more insights need to be deeply investigated in future work, we think this work will give some guidance in controlling the enanotioselectivity of LaA enantiomer directly from renewable lignocelluloses. The insights in this work provide some clues for the development of new synthetic strategies to produce chiral compounds, that is, enantioselective production of chiral molecule can be achieved by controlling the interaction of the reactants with an achiral catalyst. The information in the present work can also help us to understand the formation mechanism of chiral compounds in nature.

Limitations of the Study

The ee value of D-LaA needs further improvement, although a little more D-enantiomer can be obtained from biomass by chemocatalysis. This increases the difficulty of separation and purification of LaA enantiomers. It is therefore necessary to design chiral catalysts/ligands to improve the enantioselectivity in further work.

METHODS

All methods can be found in the accompanying Transparent Methods supplemental file.

SUPPLEMENTAL INFORMATION

Supplemental Information includes Transparent Methods, 33 figures, 2 schemes, 11 tables, and 2 notes and can be found with this article online at https://doi.org/10.1016/j.isci.2019.01.008.

AUTHOR CONTRIBUTIONS

S.X., Y.W., and Y.X. performed all the experiments; S.X. and Jinamei Li analyzed the experimental data. S.X. and Jing Li conducted the theoretical computations and analyzed the data. Jianmei Li reviewed and co-wrote the manuscript. C.H. designed the study, analyzed all the experimental results, and reviewed and co-wrote the paper.

DECLARATION OF INTERESTS

Part of the results of this article (the catalytic system) was used to apply for a Chinese patent (Application number, 201810868191.1). The authors declare no other competing interests.

iScience

CellPress

REFERENCES

Abdel-Rahman, M.A., Tashiro, Y., and Sonomoto, K. (2013). Recent advances in lactic acid production by microbial fermentation processes. Biotechnol. Adv. *31*, 877–902.

Baek, S.H., Kwon, E.Y., Kim, Y.H., and Hahn, J.S. (2016). Metabolic engineering and adaptive evolution for efficient production of D-lactic acid in Saccharomyces cerevisiae. Appl. Microbiol. Biotechnol. *100*, 2737–2748.

Besson, M., Gallezot, P., and Pinel, C. (2014). Conversion of biomass into chemicals over metal catalysts. Chem. Rev. *114*, 1827–1870.

Castillo Martinez, F.A., Balciunas, E.M., Salgado, J.M., Domínguez González, J.M., Converti, A., and Oliveira, R.P.D.S. (2013). Lactic acid properties, applications and production: a review. Trends Food Sci. Tech. *30*, 70–83.

Chen, Y., Geever, L.M., Killion, J.A., Lyons, J.G., Higginbotham, C.L., and Devine, D.M. (2016). Review of multifarious applications of poly (lactic acid). J. Macromol. Sci. Polym. Rev. *55*, 1057–1075.

Coman, S.M., Verziu, M., Tirsoaga, A., Jurca, B., Teodorescu, C., Kuncser, V., Parvulescu, V.I., Scholz, G., and Kemnitz, E. (2015). NbF$_5$–AlF$_3$ catalysts: design, synthesis, and application in lactic acid synthesis from cellulose. ACS Catal. *5*, 3013–3026.

Dapsens, P.Y., and Mondelli, C. (2015). Design of Lewis-acid centres in zeolitic matrices for the conversion of renewables. Chem. Soc. Rev. *44*, 7025–7043.

Davachi, S.M., and Kaffashi, B. (2015). Polylactic acid in medicine. Polym. Plast. Technol. Eng. *54*, 944–967.

Delidovich, I., Hausoul, P.J., Deng, L., Pfutzenreuter, R., Rose, M., and Palkovits, R. (2016). Alternative monomers based on lignocellulose and their use for polymer production. Chem. Rev. *116*, 1540–1599.

Deng, W., Wang, P., Wang, B., Wang, Y., Yan, L., Li, Y.Y., Zhang, Q., Cao, Z., and Wang, Y. (2018). Transformation of cellulose and related carbohydrates into lactic acid with bifunctional Al(III)-Sn(II) catalysts. Green Chem. *20*, 735–744.

Desguin, B., Goffin, P., Viaene, E., Kleerebezem, M., Martin-Diaconescu, V., Maroney, M.J., Declercq, J.P., Soumillion, P., and Hols, P. (2014). Lactate racemase is a nickel-dependent enzyme activated by a widespread maturation system. Nat. Commun. *5*, 3615.

Dong, W., Shen, Z., Peng, B., Gu, M., Zhou, X., Xiang, B., and Zhang, Y. (2016). Selective chemical conversion of sugars in aqueous solutions without alkali to lactic acid over a Zn-Sn-beta lewis acid-base catalyst. Sci. Rep. *6*, 26713.

Dusselier, M., and Sels, B.F. (2014). Selective catalysis for cellulose conversion to lactic acid and other alpha-hydroxy acids. Top. Curr. Chem. *353*, 85–125.

Dusselier, M., Van Wouwe, P., Dewaele, A., Makshina, E., and Sels, B.F. (2013). Lactic acid as a platform chemical in the biobased economy: the role of chemocatalysis. Energy Environ. Sci. *6*, 1415–1442.

Ennaert, T., Van, A.J., Dijkmans, J., De, C.R., Schutyser, W., Dusselier, M., Verboekend, D., and Sels, B.F. (2016). Potential and challenges of zeolite chemistry in the catalytic conversion of biomass. Chem. Soc. Rev. *47*, 584–611.

Eş, I., Mousavi, A.K., Barba, F.J., Saraiva, J.A., Sant'Ana, A.S., and Hashemi, S. (2018). Recent advancements in lactic acid production-a review. Food Res. Int. *103*, 763–770.

Farrán, A., Cai, C., Sandoval, M., Xu, Y., Liu, J., Hernáiz, M.J., and Linhardt, R.J. (2015). Green solvents in carbohydrate chemistry: from raw materials to fine chemicals. Chem. Rev. *115*, 6811–6853.

Feng, J., Holmes, M., and Krische, M.J. (2017). Acyclic quaternary carbon stereocenters via enantioselective transition metal catalysis. Chem. Rev. *117*, 12564–12580.

Gallezot, P. (2012). Conversion of biomass to selected chemical products. Chem. Soc. Rev. *43*, 1538–1558.

Holm, M.S., and Taarning, E. (2010). Conversion of sugars to lactic acid derivatives using heterogeneous zeotype catalysts. Science *328*, 602–605.

Holm, M.S., Pagántorres, Y.J., Saravanamurugan, S., Riisager, A., Dumesic, J.A., and Taarning, E. (2012). Sn-Beta catalysed conversion of hemicellulosic sugars. Green Chem. *14*, 702–706.

Lasprilla, A.J., Martinez, G.A., Lunelli, B.H., Jardini, A.L., and Filho, R.M. (2012). Poly-lactic acid synthesis for application in biomedical devices-a review. Biotechnol. Adv. *30*, 321–328.

Li, L., Shen, F., Smith, R.L., and Qi, X. (2017). Quantitative chemocatalytic production of lactic acid from glucose under anaerobic conditions at room temperature. Green Chem. *19*, 76–81.

Lin, C.S.K., Pfaltzgraff, L.A., Herrerodavila, L., Mubofu, E.B., Abderrahim, S., Clark, J.H., Koutinas, A.A., Kopsahelis, N., Stamatelatou, K., and Dickson, F. (2013). Food waste as a valuable resource for the production of chemicals, materials and fuels: current situation and global perspective. Energy Environ. Sci. *6*, 426–464.

Liu, W.J., Li, W.W., Jiang, H., and Yu, H.Q. (2017). Fates of chemical elements in biomass during its pyrolysis. Chem. Rev. *117*, 6367–6398.

Maki-Arvela, P., Simakova, I.L., Salmi, T., and Murzin, D.Y. (2014). Production of lactic acid/lactates from biomass and their catalytic transformations to commodities. Chem. Rev. *114*, 1909–1971.

Mäkiarvela, P., Salmi, T., Holmbom, B., Willför, S., and Murzin, D.Y. (2011). Synthesis of sugars by hydrolysis of hemicelluloses-a review. Chem. Rev. *111*, 5638–5666.

Nagarajan, V., Mohanty, A.K., and Misra, M. (2016). Perspective on polylactic acid (PLA) based sustainable materials for durable applications: focus on toughness and heat resistance. ACS Sustain. Chem. Eng. *4*, 2899–2916.

Otocka, S., Kwiatkowska, M., Madalińska, L., and Kiełbasiński, P. (2017). Chiral organosulfur ligands/catalysts with a stereogenic sulfur atom: applications in asymmetric synthesis. Chem. Rev. *117*, 4147–4181.

Pescarmona, P.P., Janssen, K.P.F., Delaet, C., Stroobants, C., Houthoofd, K., An, P., Jonghe, C.D., Paul, J.S., Jacobs, P.A., and Sels, B.F. (2010). Zeolite-catalysed conversion of C3 sugars to alkyl lactates. Green Chem. *12*, 1083–1089.

Rasrendra, C.B., Makertihartha, I.G.B.N., Adisasmito, S., and Heeres, H.J. (2010). Green chemicals from d-glucose: systematic studies on catalytic effects of inorganic salts on the chemo-selectivity and yield in aqueous solutions. J. Top. Catal. *53*, 1241–1247.

Román-Leshkov, Y., Moliner, M., Labinger, J.A., and Davis, M.E. (2010). Mechanism of glucose isomerization using a solid lewis acid catalyst in water. Angew. Chem. Int. Ed. *49*, 9138–9141.

Schneebeli, S.T., Hall, M.L., Breslow, R., and Friesner, R. (2009). Quantitative DFT modeling of the enantiomeric excess for dioxirane-catalyzed epoxidations. J. Am. Chem. Soc. *131*, 3965–3973.

Sharninghausen, L.S., Campos, J., Manas, M.G., and Crabtree, R.H. (2014). Efficient selective and atom economic catalytic conversion of glycerol to lactic acid. Nat. Commun. *5*, 5084.

Tuck, C.O., Pérez, E., Horváth, I.T., Sheldon, R.A., and Poliakoff, M. (2012). Valorization of biomass: deriving more value from waste. Science *337*, 695–699.

Wang, Y., Deng, W., Wang, B., Zhang, Q., Wan, X., Tang, Z., Wang, Y., Zhu, C., Cao, Z., Wang, G., and Wan, H. (2013). Chemical synthesis of lactic acid from cellulose catalysed by lead(II) ions in water. Nat. Commun. *4*, 2141.

Yang, L., Su, J., Carl, S., Lynam, J.G., Yang, X., and Lin, H. (2015). Catalytic conversion of hemicellulosic biomass to lactic acid in pH neutral aqueous phase media. Appl. Catal. B Environ. *162*, 149–157.

Yang, L., Yang, X., Tian, E., Vattipalli, V., Fan, W., and Lin, H. (2016a). Mechanistic insights into the production of methyl lactate by catalytic conversion of carbohydrates on mesoporous Zr-SBA-15. J. Catal. *333*, 207–216.

Yang, G.Y., Ke, Y.H., Ren, H.F., Liu, C.L., Yang, R.Z., and Dong, W.S. (2016b). The conversion of glycerol to lactic acid catalyzed by ZrO$_2$-supported CuO catalysts. Chem. Eng. J. *283*, 759–767.

Zhang, Z., Song, J., and Han, B. (2017). Catalytic transformation of lignocellulose into chemicals and fuel products in ionic liquids. Chem. Rev. *117*, 6834–6880.

Supplemental Information

D-Excess-LaA Production Directly

from Biomass by Trivalent Yttrium Species

Shuguang Xu, Jing Li, Jianmei Li, Yi Wu, Yuan Xiao, and Changwei Hu
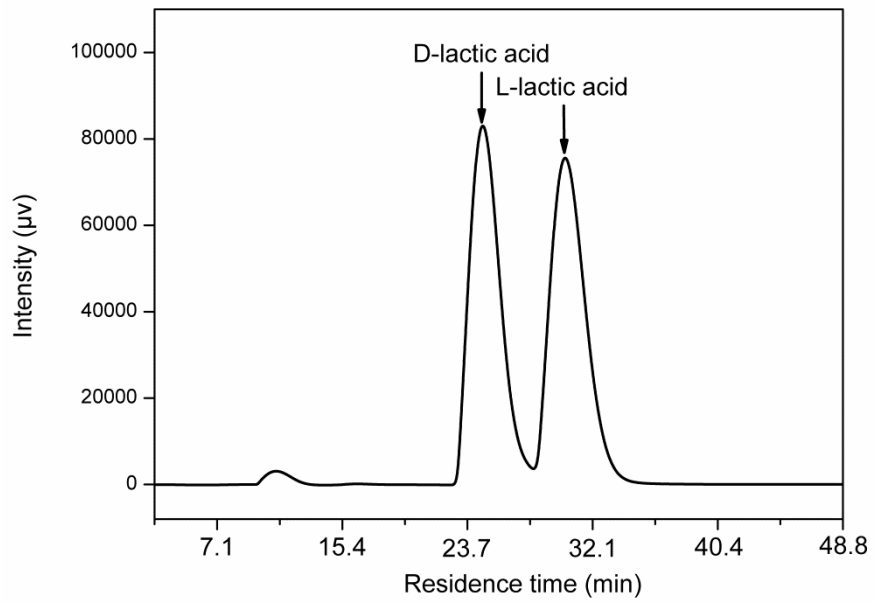
Figure S1. The HPLC analysis results of the mixture of D/L-lactic acid, Related to Table 1.
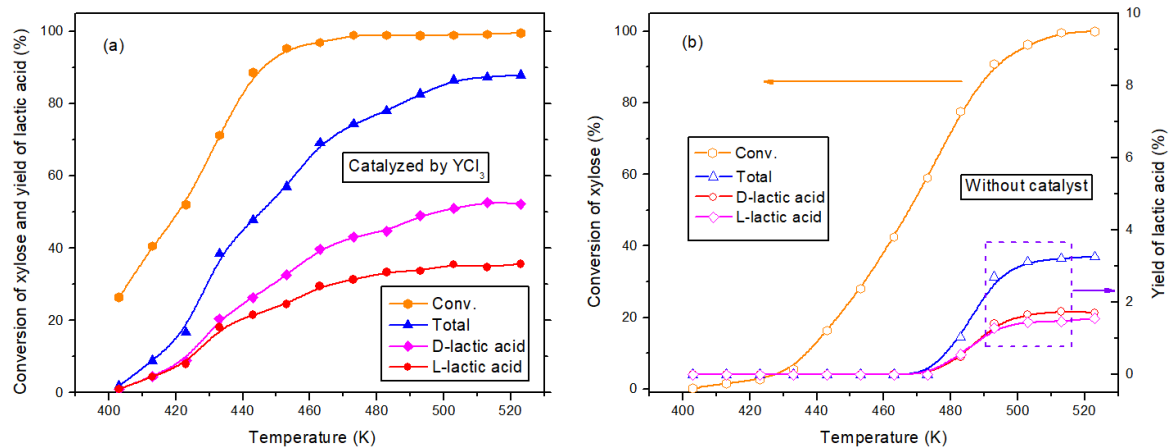
Figure S2. The conversion of xylose to lactic acid (a) catalyzed by YCl₃, (b) without catalyst. Reaction conditions: 0.20 g (26.7 mM) xylose; 50 mL H_2O; 6.6 mM YCl_3; 2 MPa N_2, reaction time 0.5 h, Related to Table 1.
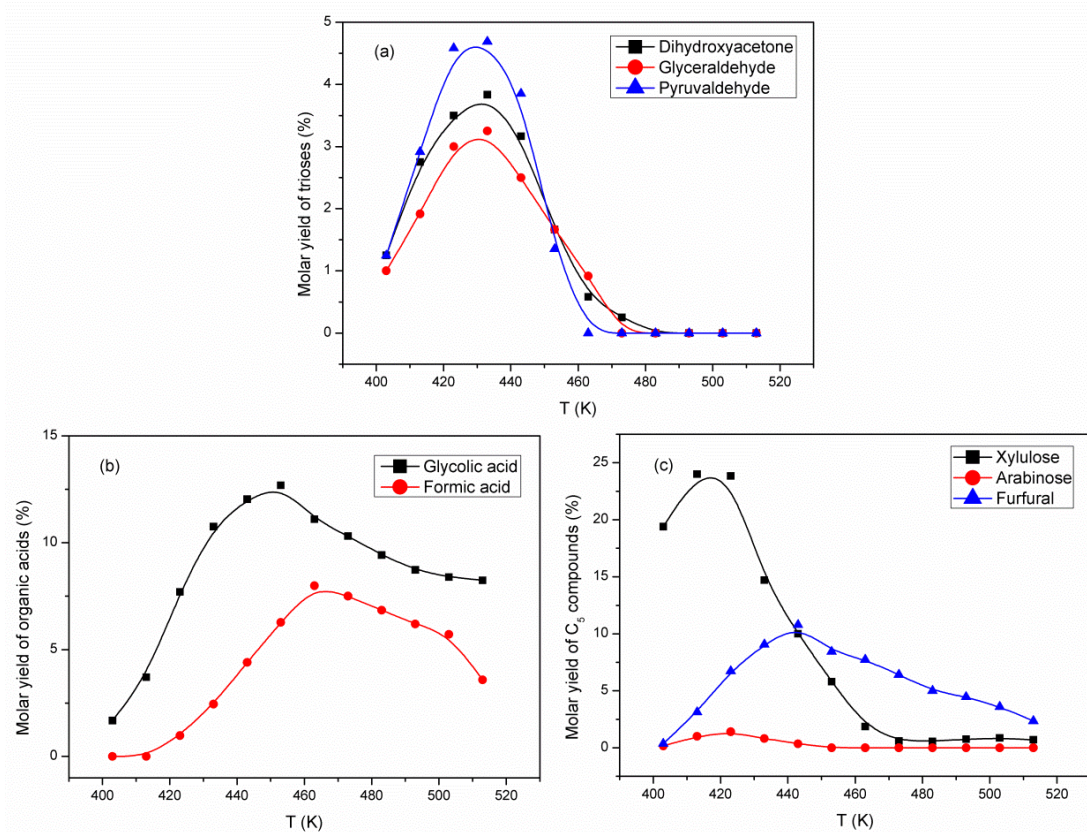
Figure S3. Effect of temperature on the yield of (a) trioses, (b) organic acid, (c) C_5 compounds derived from xylose conversion in the presence of YCl_3. Reaction conditions: 0.20 g xylose (26.7 mM); 50 mL H_2O; 6.6 mM YCl_3; N_2, 2 MPa; reaction time, 0.5 h, Related to Table 1.
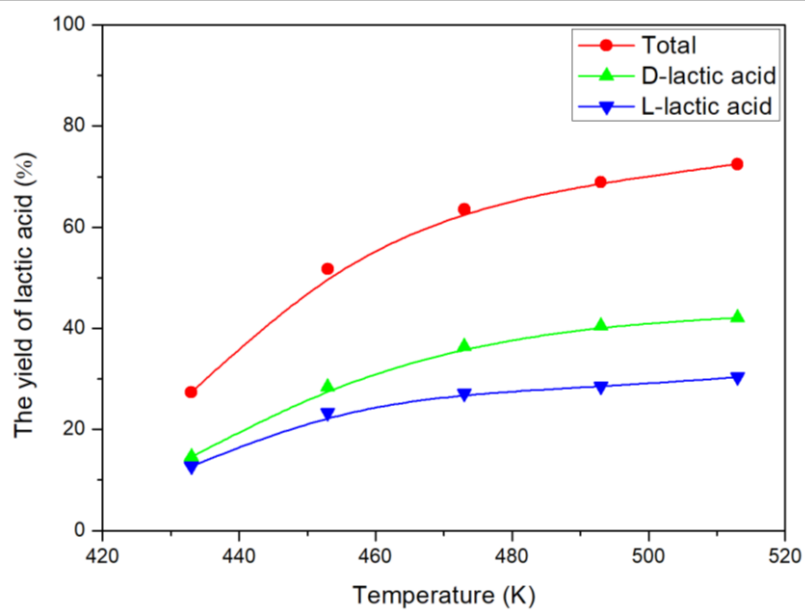
Figure S4. The yield of lactic acid from xylan in the presence of diluted Y(Ⅲ). Reaction conditions: 0.20 g xylan; 50 mL H_2O; 6.6 mM YCl_3; N_2, 2 MPa; reaction time, 0.5 h, Related to Table 1.
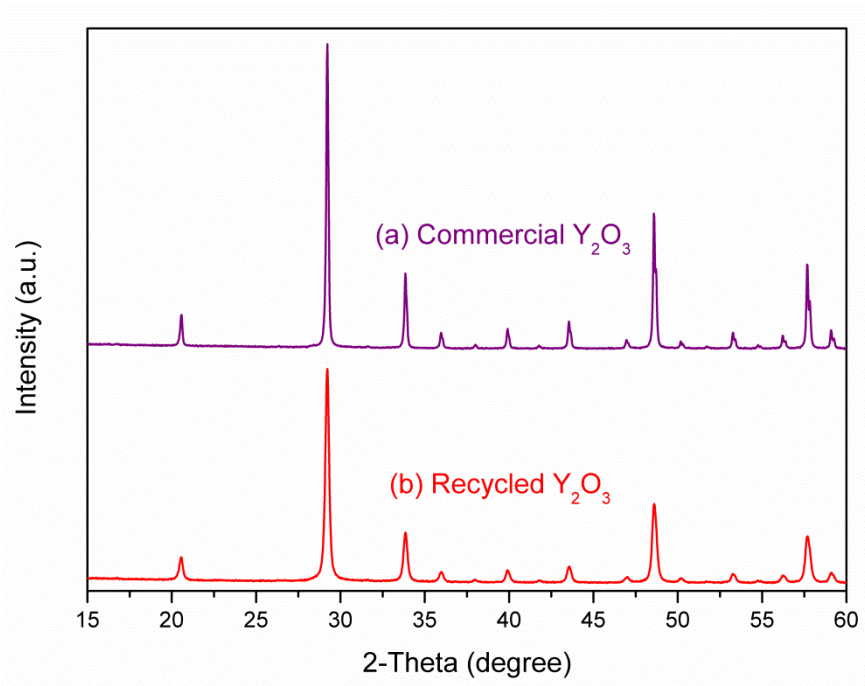
Figure S5. The XRD patterns of (a) commercial Y_2O_3, (b) recovered Y_2O_3, Related to Table 1.
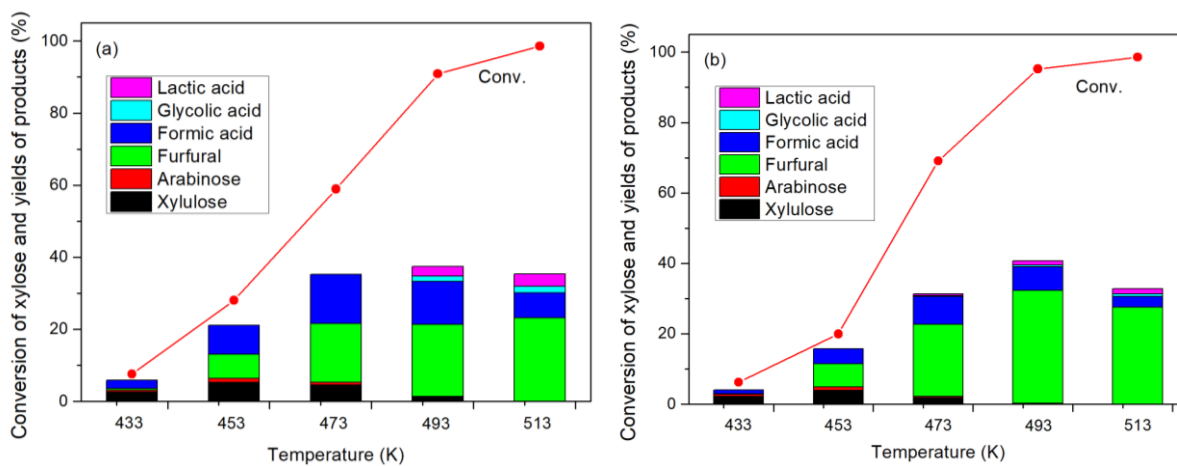
Figure S6. Conversion of xylose at different temperatures (a) without catalyst, (b) HCl as the catalyst with the similar initial pH value to that of diluted YCl₃ aqueous solution. Reaction conditions: 0.20 g xylose (26.7 mM); 50 mL H_2O; N_2, 2 MPa; reaction time, 0.5 h, Related to Table 1.
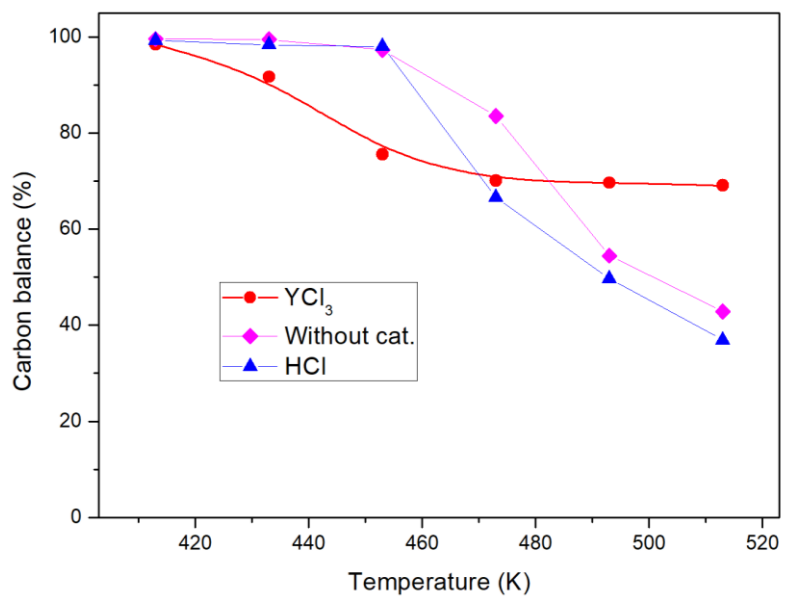
Figure S7. The carbon balance in the conversion of xylose. Reaction conditions: 0.20 g xylose (26.7m M); 50 mL H_2O; 6.6 mM YCl_3 or without catalyst; N_2, 2 MPa; reaction time, 0.5 h, Related to Table 1.
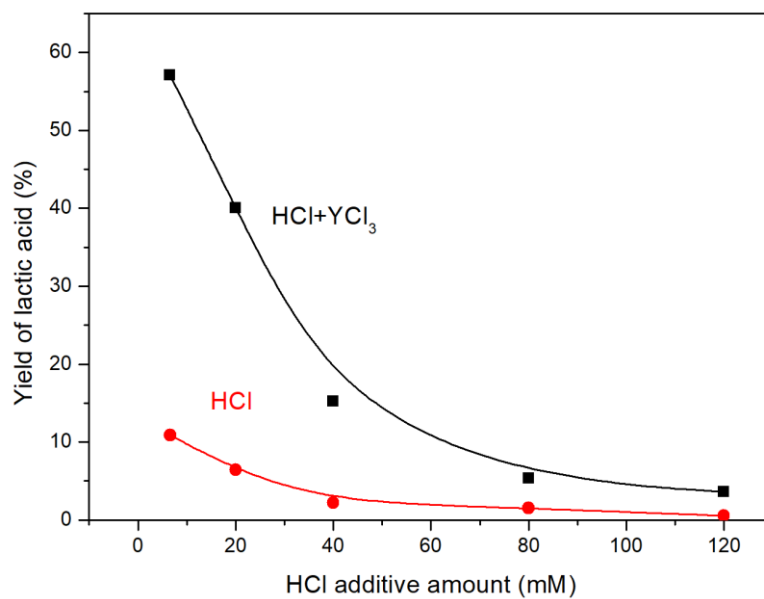
Figure S8. The influence of HCl amount on the yield of lactic acid from xylose. Reaction conditions: 0.20 g (26.7 mM) xylose; 6.6 mM YCl$_3$; 50 mL H$_2$O; reaction time, 0.5 h; temperature, 493 K, Related to Figure 1.
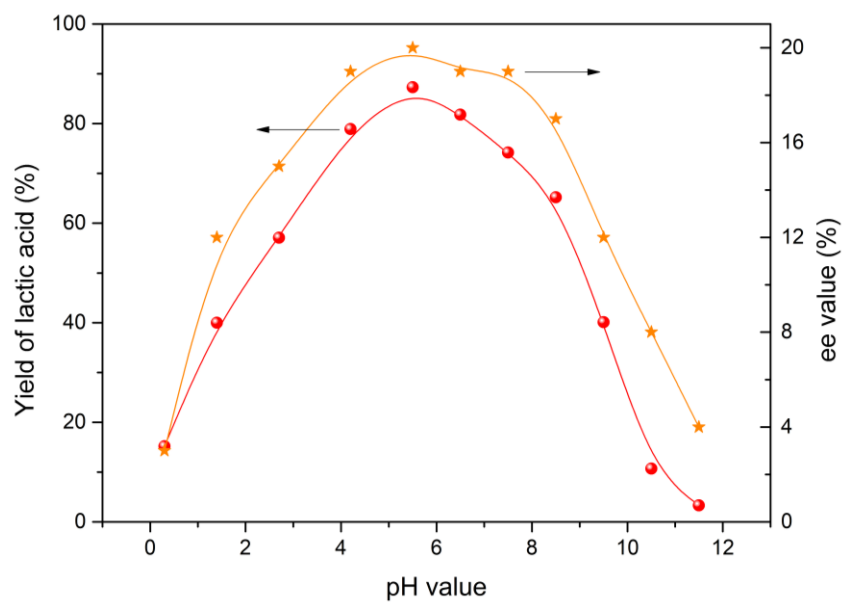
Figure S9. The influence of the pH value on the conversion of xylose to lactic acid in the presence of diluted Y(Ⅲ). Reaction conditions: 0.20 g xylose; 50 mL H_2O; 6.6 mM YCl_3; N_2, 2 MPa; reaction time, 0.5 h. HCl and NaOH is used to adjust the pH value, Related to Figure 1.
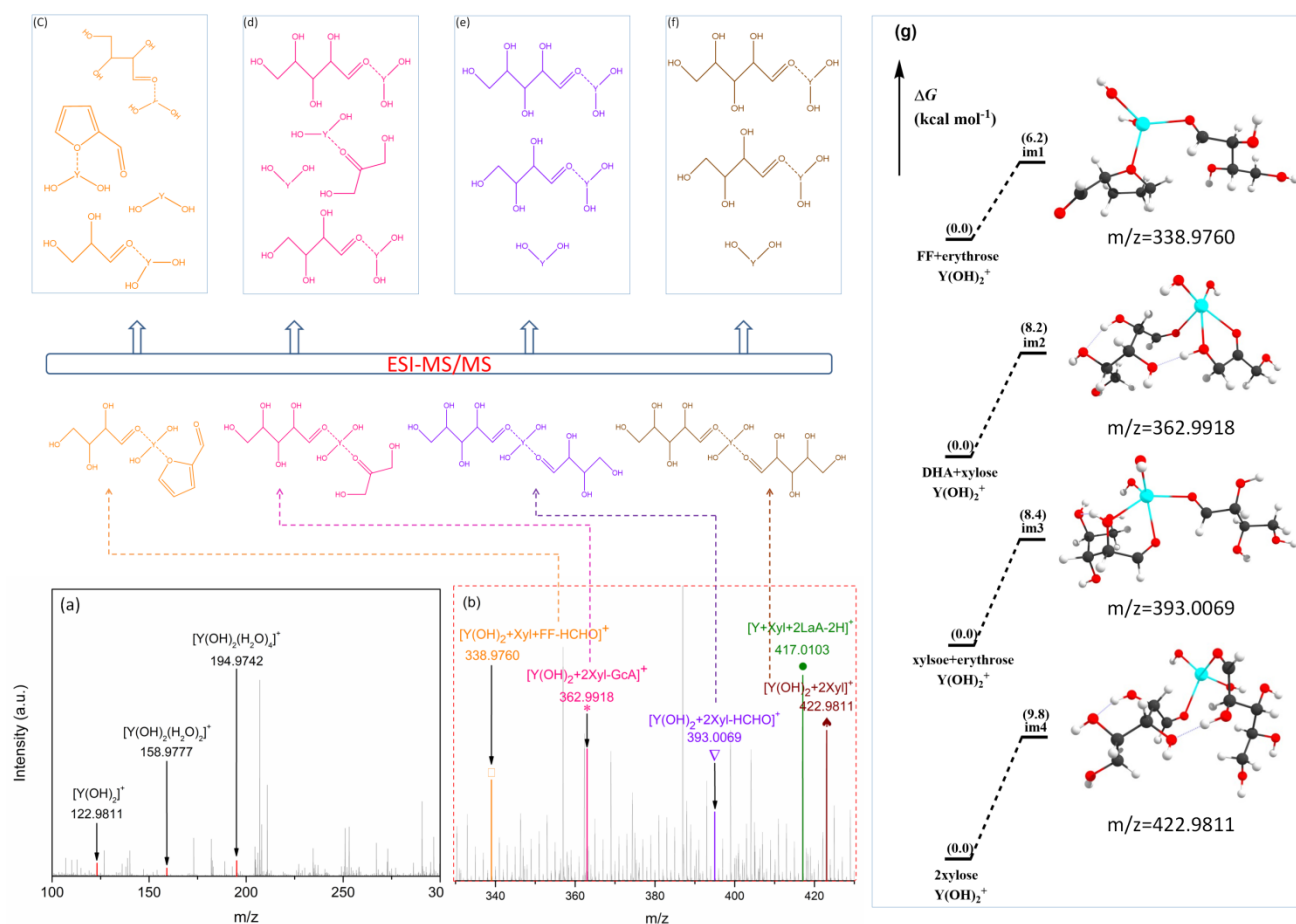
Figure S10. ESI-MS and ESI-MS/MS spectra (Positive ion mode) of YCl₃ aqueous solution (a) without xylose, (b) with xylose (m/z=330-430)), (c) the chemical structures of intermediate and its main fragments with m/z=338.9760, (d) the chemical structures of intermediate and its main fragments with m/z=362.9918, (e) the chemical structures of intermediate and its main fragments with m/z=393.0069, (f) the chemical structures of intermediate and its main fragments with m/z=422.9811, (g) four calculated relative Gibbs energy profiles (in kcal·mol⁻¹) of species captured in Fig. S7b. Xyl represents xylose, GcA represents glycolic aldehyde, FF represents furfural. Reaction conditions: 0.20 g (26.7 mM) xylose; 50 mL H₂O; 6.6 mM YCl₃; 423K; 0.5 h, Related to Figure 1.
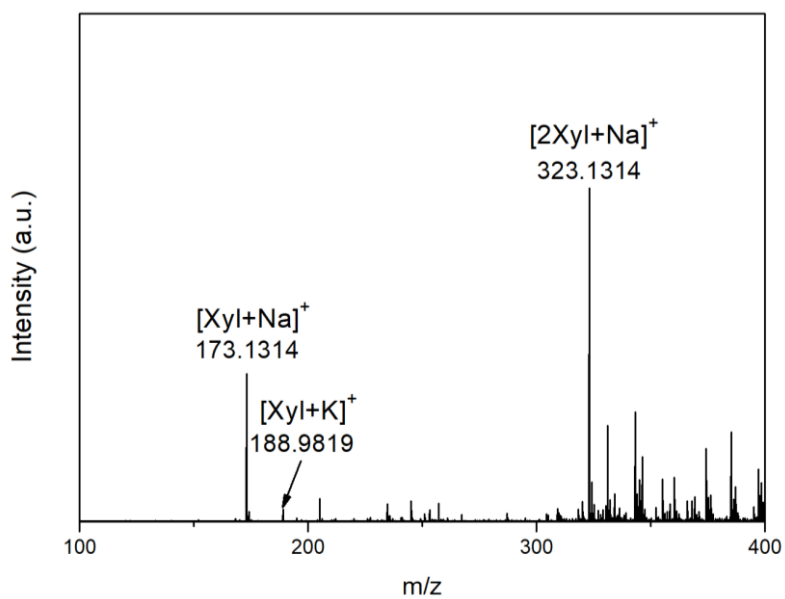
Figure S11. ESI-MS spectra of xylose aqueous solution at room temperature, Related to Figure 1.
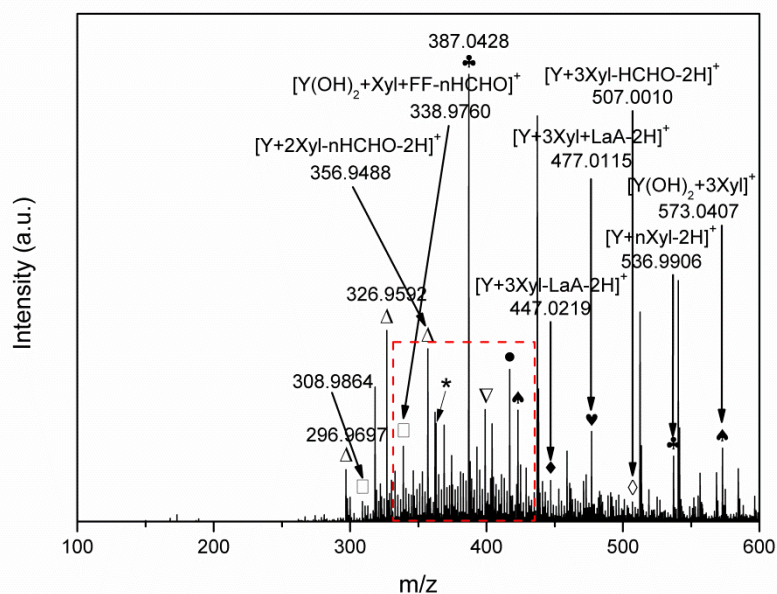
Figure S12. ESI-MS spectra of the reaction solution of xylose conversion in the presence of YCl₃. Some legends: solid club (♣), $[Y+nXyl-2H]^+$ (n=2-3); Solid Spade (♠),$[Y(OH)_2+nXyl]^+$ (n=2-3); purple open triangle (Δ), $[Y+2Xyl-nHCHO-2H]^+$ (n=1-3); open square (□), $[Y(OH)_2+Xyl+FF-nHCHO]^+$ (n=2). Xyl represents xylose; GcA represents glycolic aldehyde. Reaction conditions: 0.20 g (26.7 mM) xylose; 50 mL H_2O; 6.6 mM YCl₃; 423K, Related to Figure 1.

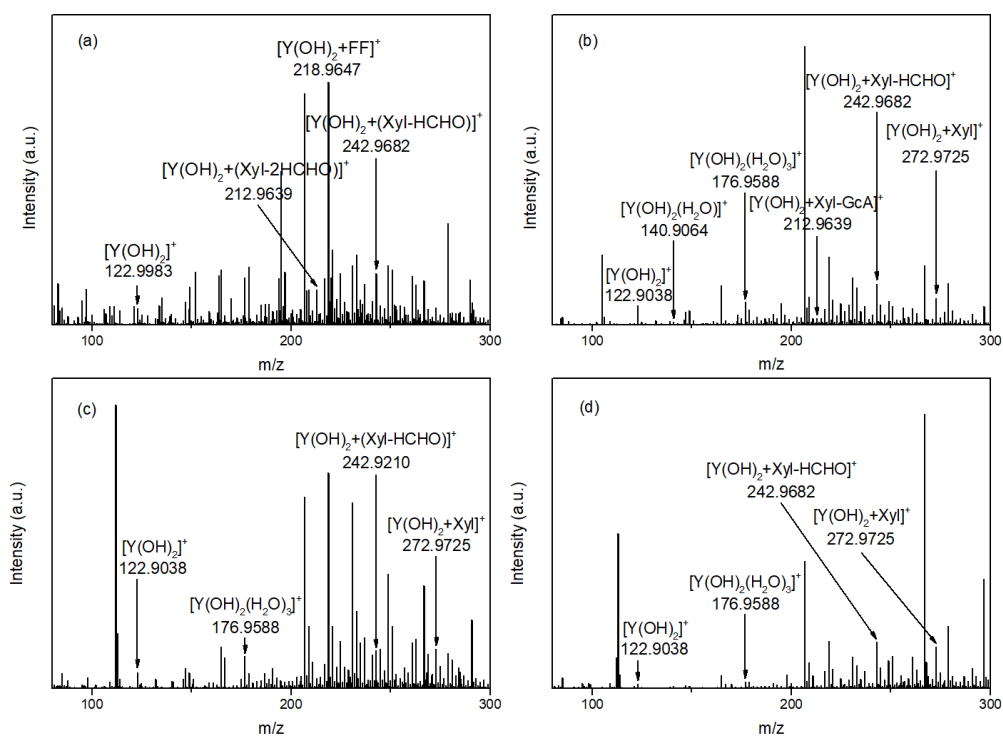**Figure S13. Electron spin ionization-mass spectroscopy/ mass spectroscopy (ESI-MS/MS) spectra of the selected peaks in Fig. 2a ((a) m/z=338.9770, (b) m/z=362.9918, (c) m/z=393.0069, (d) m/z=422.9811),** Related to Figure 1.
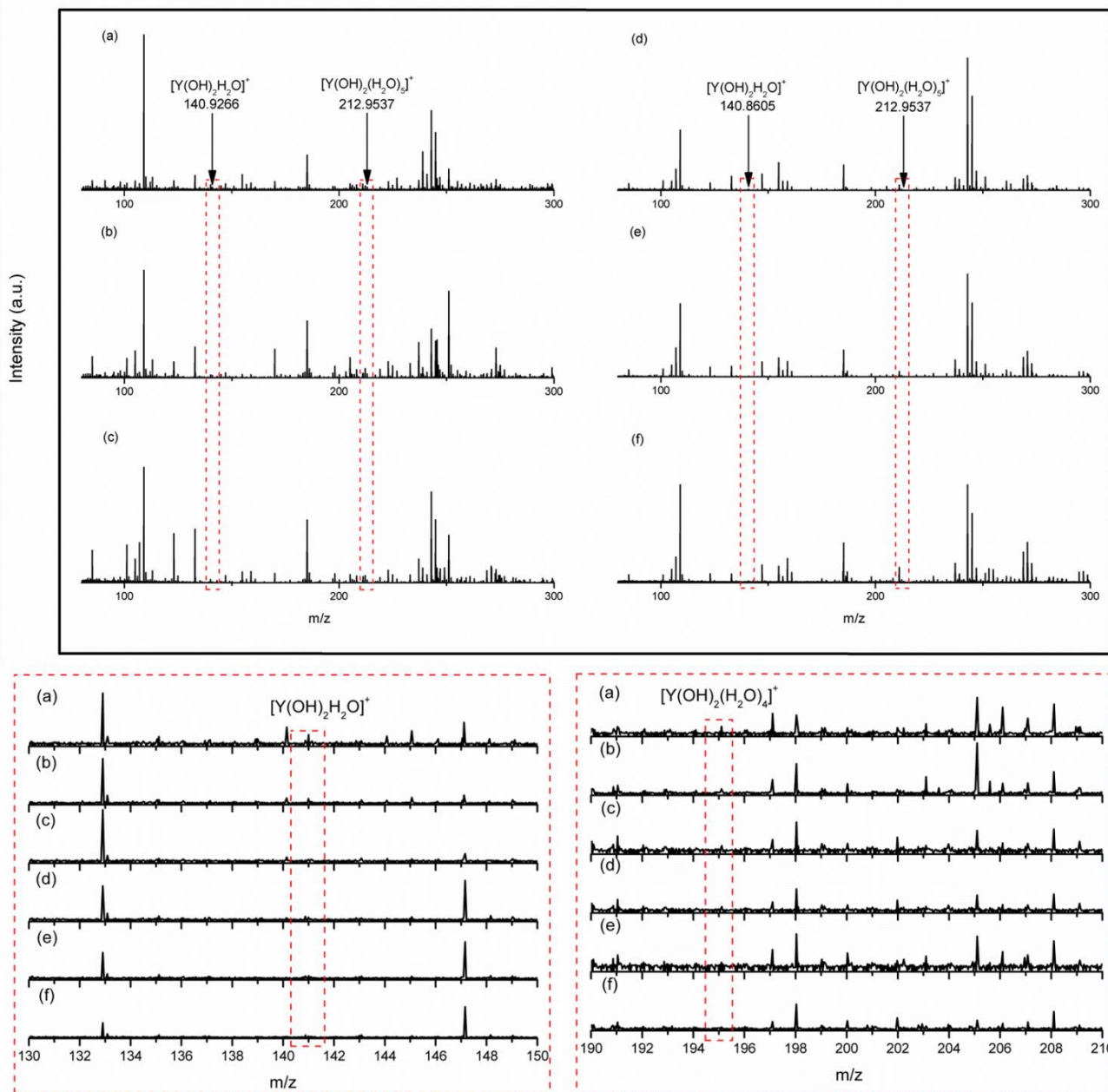
Figure S14. ESI-MS spectra of YCl₃ aqueous solution with different HCl amounts at room temperature. (a) without HCl, (b) 6.6 mM HCl, (c) 20 mM HCl, (d) 40 mM HCl, (e) 80 mM HCl, (f) 120 mM HCl, Related to Figure 1.
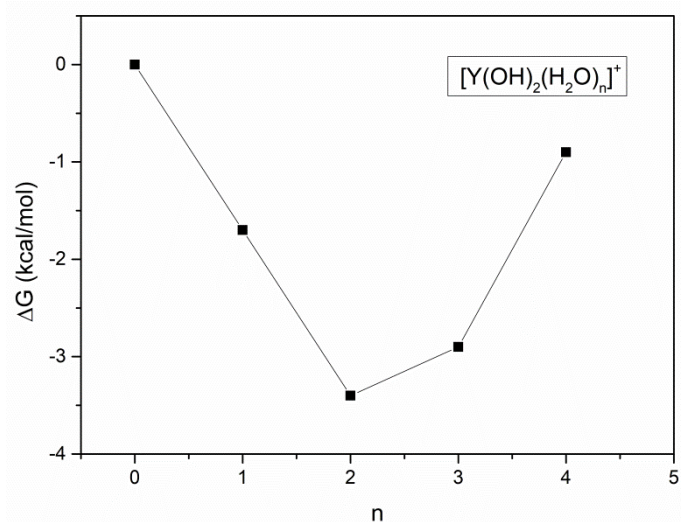
Figure S15. Aqueous Gibbs free energy (kcal mol^{-1}) as a function number of coordinating water molecule relative to the [Y(OH)$_2$(H$_2$O)$_n$]$^+$ (n=0 to 4), Related to Figure 1.
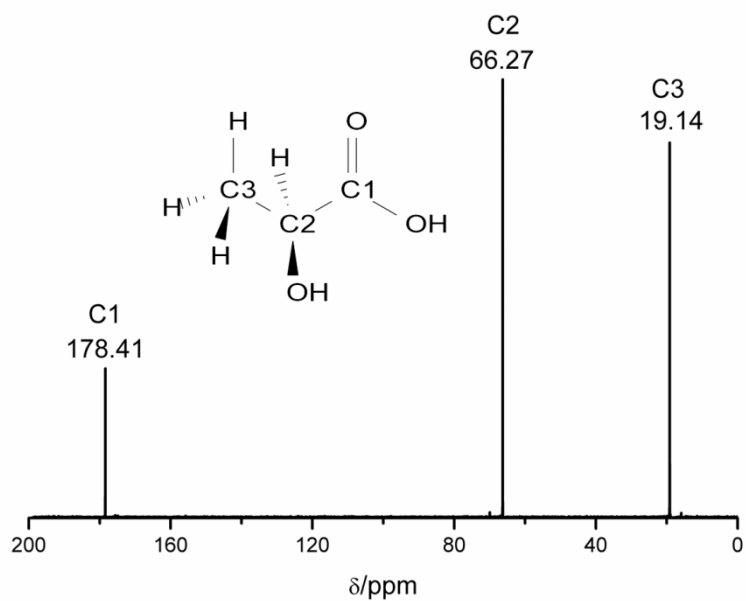
Figure S16. ^{13}C NMR spectra of lactic acid dissolved in D$_2$O, Related to Figure 1 and Figure 2.
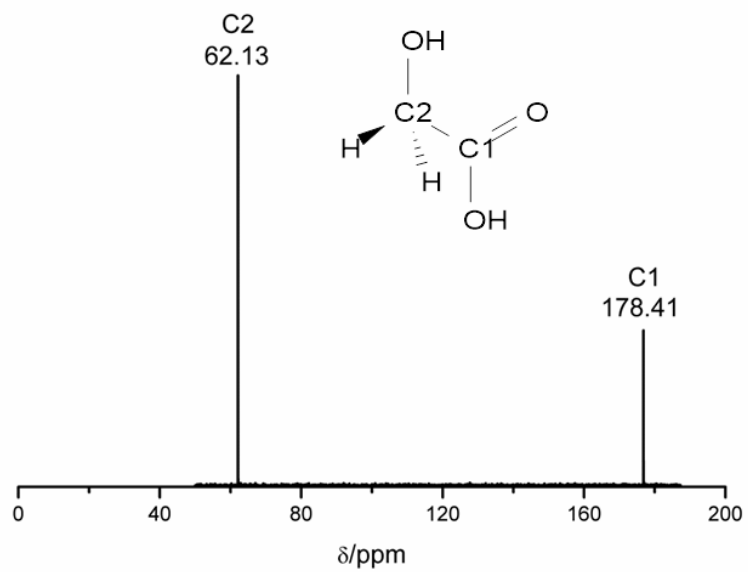
Figure S17. ^{13}C NMR spectra of glycolic acid dissolved in D$_2$O, Related to Figure 1 and Figure 2.
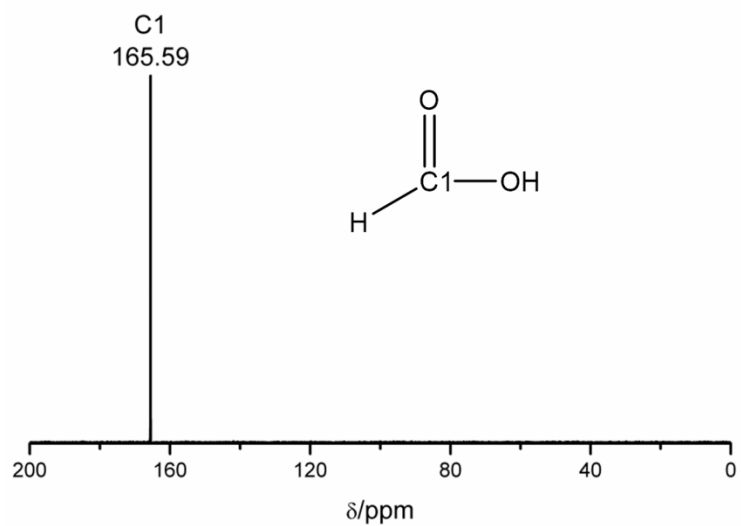
Figure S18. ^{13}**C NMR spectra of pure formic acid dissolved in D₂O,** Related to Figure 1 and Figure 2.
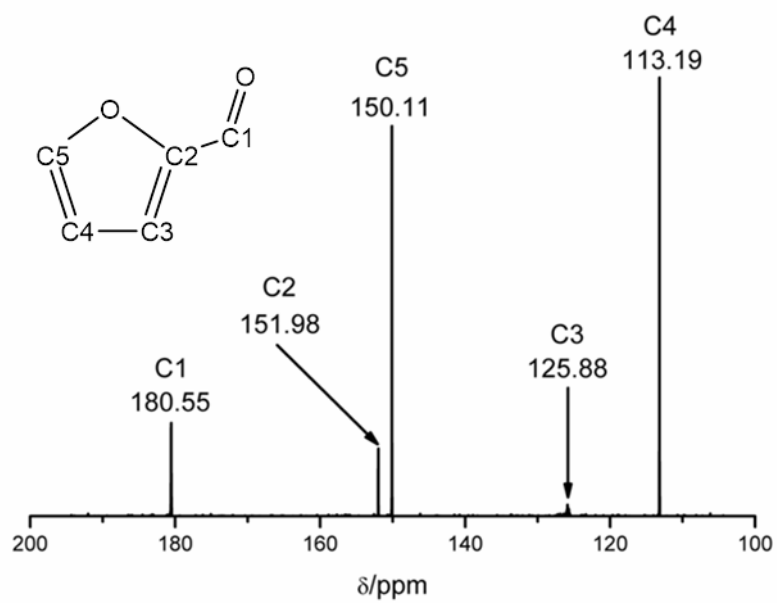
Figure S19. **^{13}C NMR spectra of pure furfural dissolved in D$_2$O,** Related to Figure 1 and Figure 2.
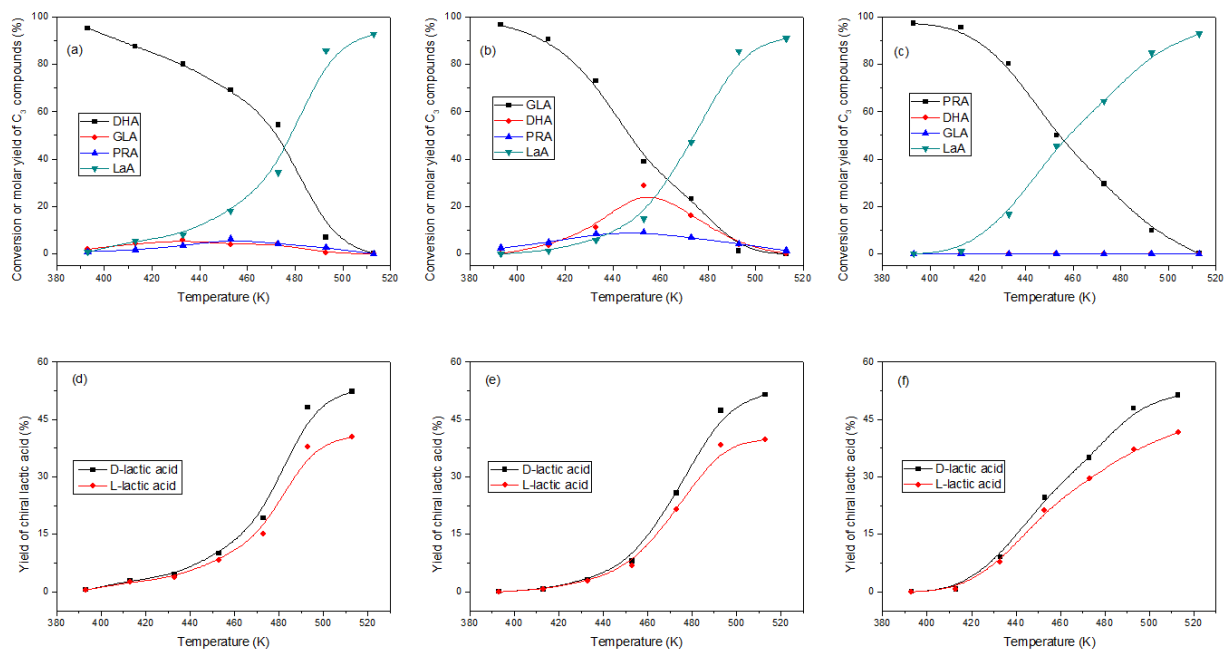
Figure S20. Catalytic performance of diluted Y(Ⅲ) ion for the conversion of (a) DHA, (b) GLA , (c) PRA to lactic acid, and the yield of lactic acid from (d) DHA, (e) GLA, (f) PRA. Reaction conditions: 0.12 g (26.7 mM) trioses; 50 mL H$_2$O; 6.6 mM YCl$_3$; N$_2$, 2 MPa; reaction time, 0.5 h, Related to Figure 2 and Figure 3.
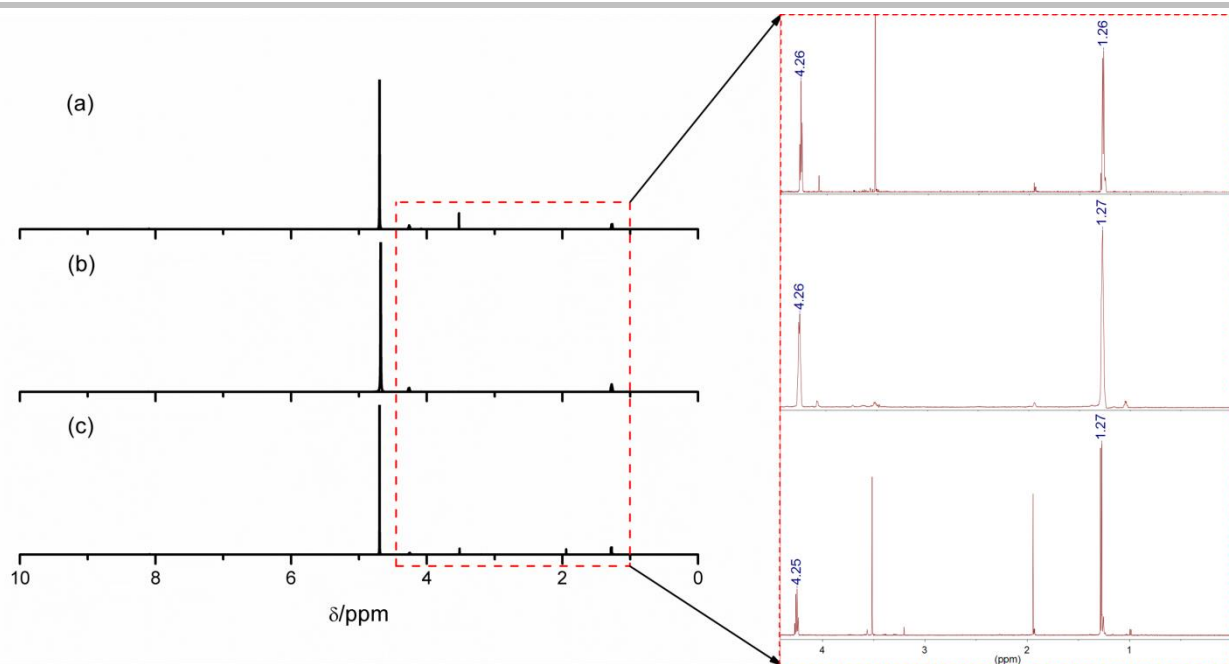
Figure S21. **^{1}HNMR spectra of the lactic acid from different trioses conversion ((a) DHA, (b) GLA, (c) PRA)) in the presence of diluted Y(Ⅲ) ion in D$_2$O.** Reaction conditions: 0.12 g (26.7 mM) trioses; 50 mL D$_2$O; 6.6 mM YCl$_3$; N$_2$, 2 MPa; reaction time, 0.5 h; temperature, 493 K, Related to Figure 1 and Figure 2.
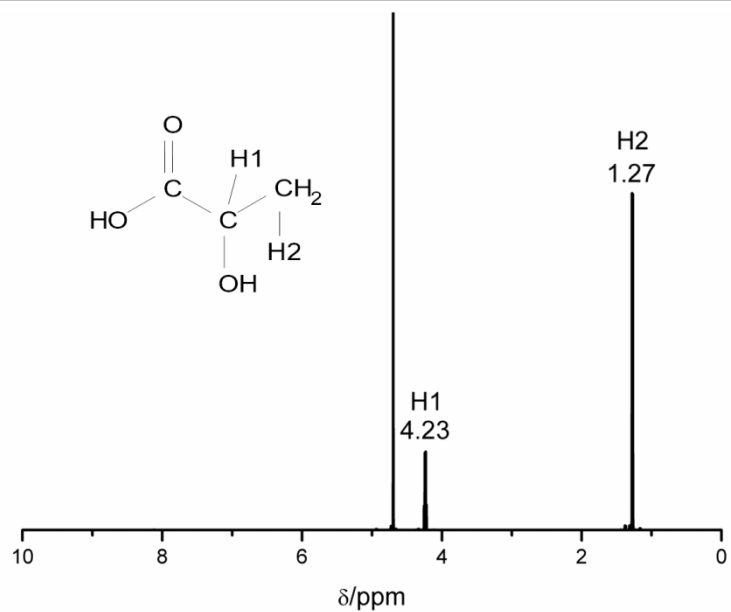
Figure S22. ¹H NMR spectra of pure lactic acid dissolved in D₂O, Related to Figure 1 and Figure 2.
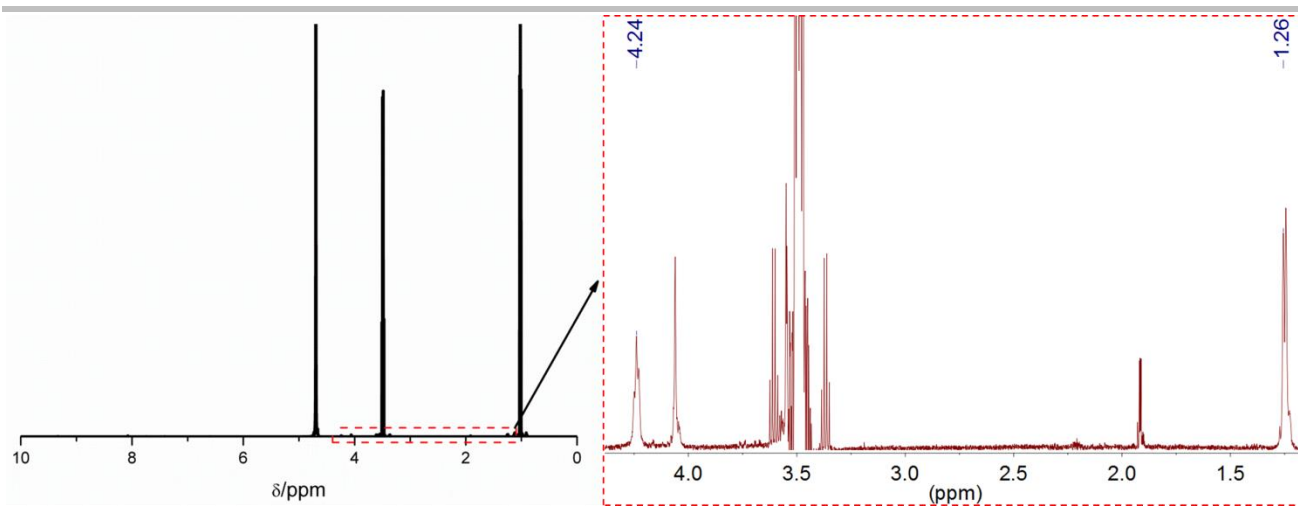
**Figure S23. ¹HNMR spectra of the liquid mixture derived from xylose conversion in the presence of Y(Ⅲ) with D₂O as solvent.** Reaction conditions: 0.20 g (26.7 mM) xylose; 50 mL D₂O; 6.6 mM YCl₃; N₂, 2 MPa; reaction time, 0.5 h; temperature, 493 K, Related to Figure 1 and Figure 2.
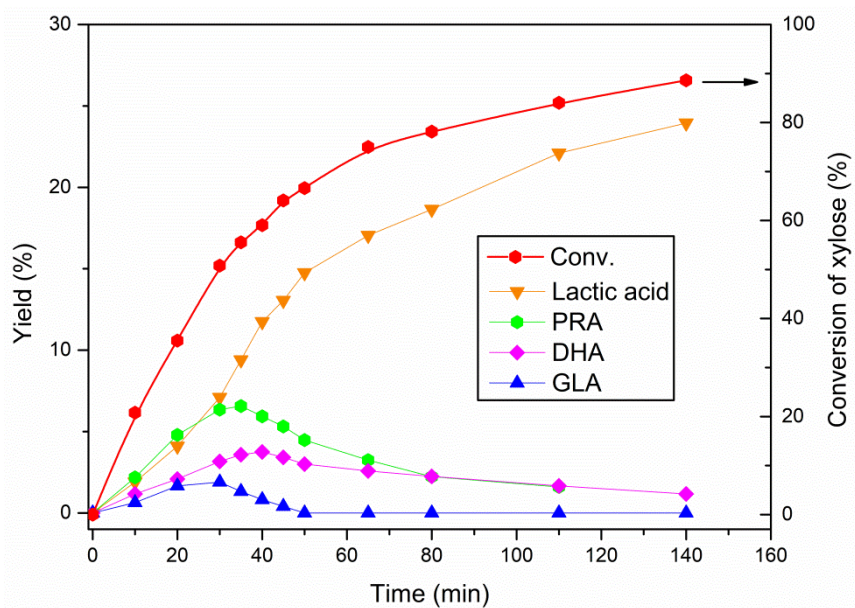
Figure S24. The influence of reaction time on the yield of liquid products for xylose conversion in the presence of Y(Ⅲ). Reaction conditions: 0.20 g (26.7 mM) xylose; 50 mL H_2O; 6.6 mM YCl_3; N_2, 2 MPa; temperature, 423 K, Related to Figure 3.
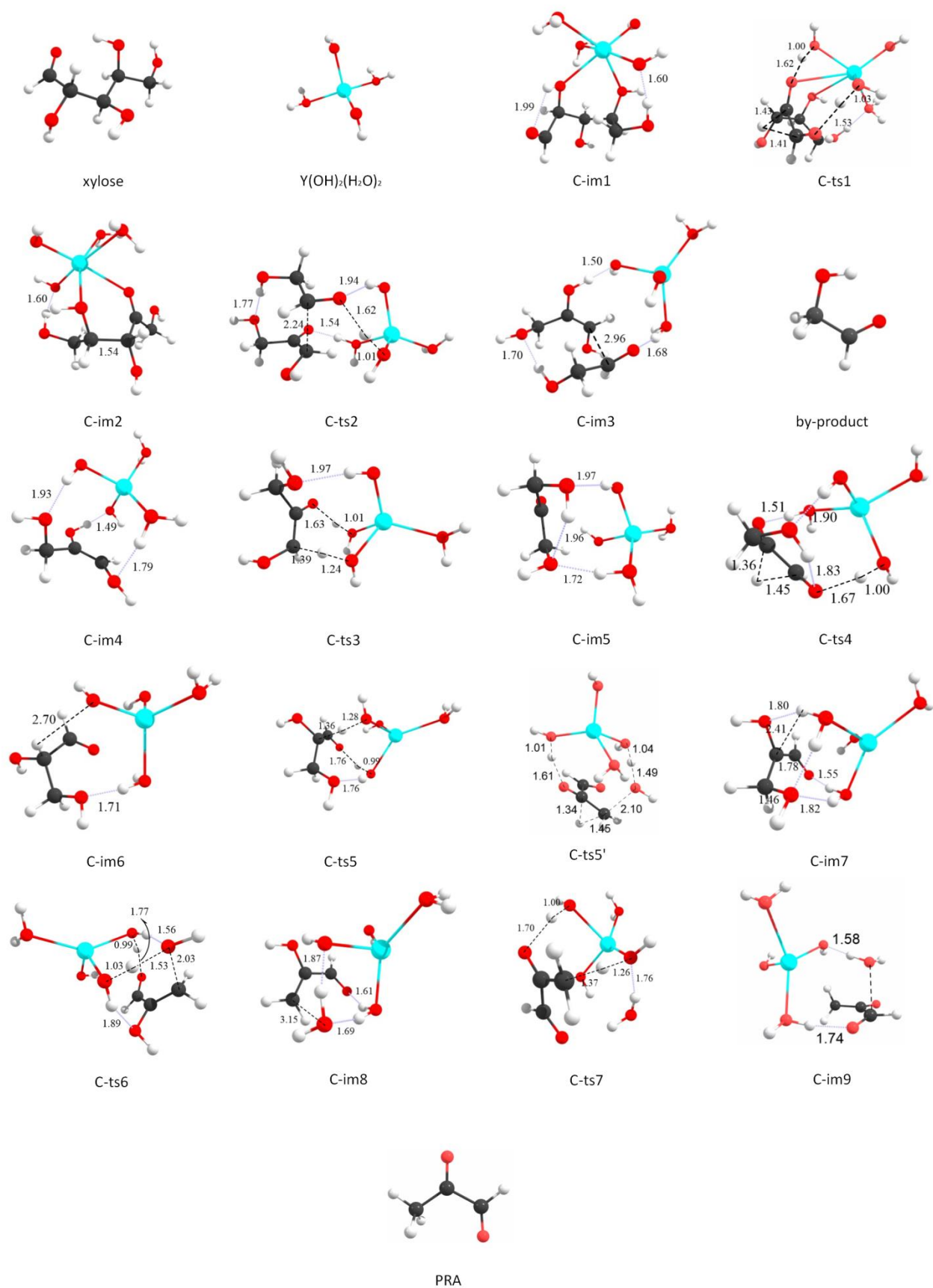
Figure S25. The optimized structures (in Å) of species for the conversion of xylose to lactic acid for the calculated relative Gibbs energy profiles (in kcal mol^{-1}) in Fig. 3b, Related to Figure 3.
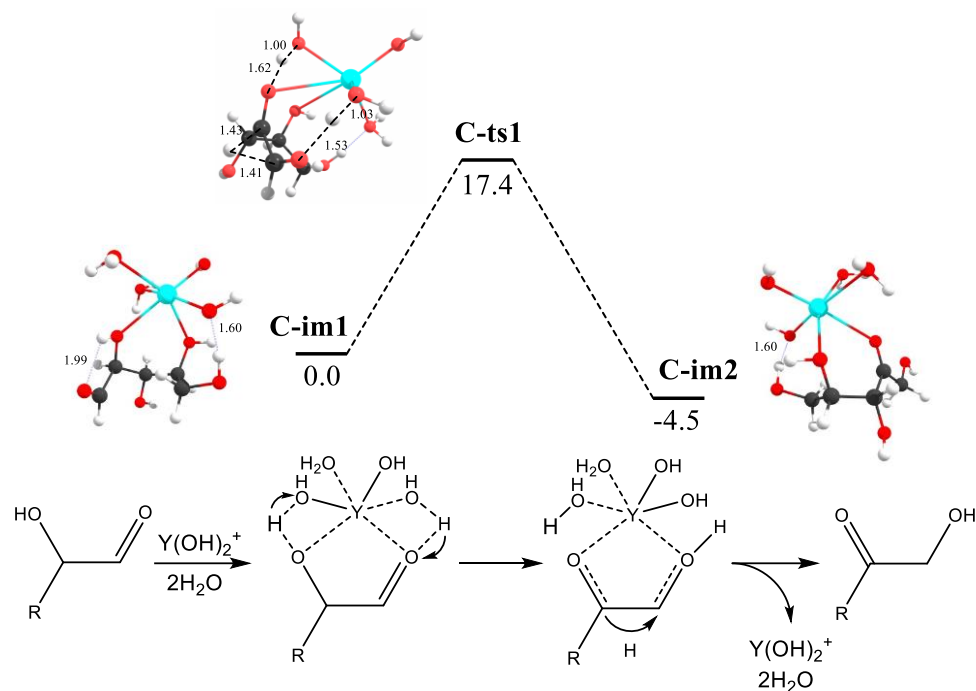
Figure S26. Energy profiles (in kcal mol $^{-1}$) and optimized structures (in Å) for the reaction pathway of the isomerization of xylose to xylulose in the presence of Y(Ⅲ). We found that the hydroxyl in $[Y(OH)_2(H_2O)_2]^+$ could deprive the hydrogen atom of C2-OH in xylose to form H_2O, and then the primary H_2O of $[Y(OH)_2(H_2O)_2]^+$ could provide a hydrogen atom to C1=O forming C1-OH. We descript this H-shift from C2-O to C1-O by passing through a water molecule, Related to Figure 3.
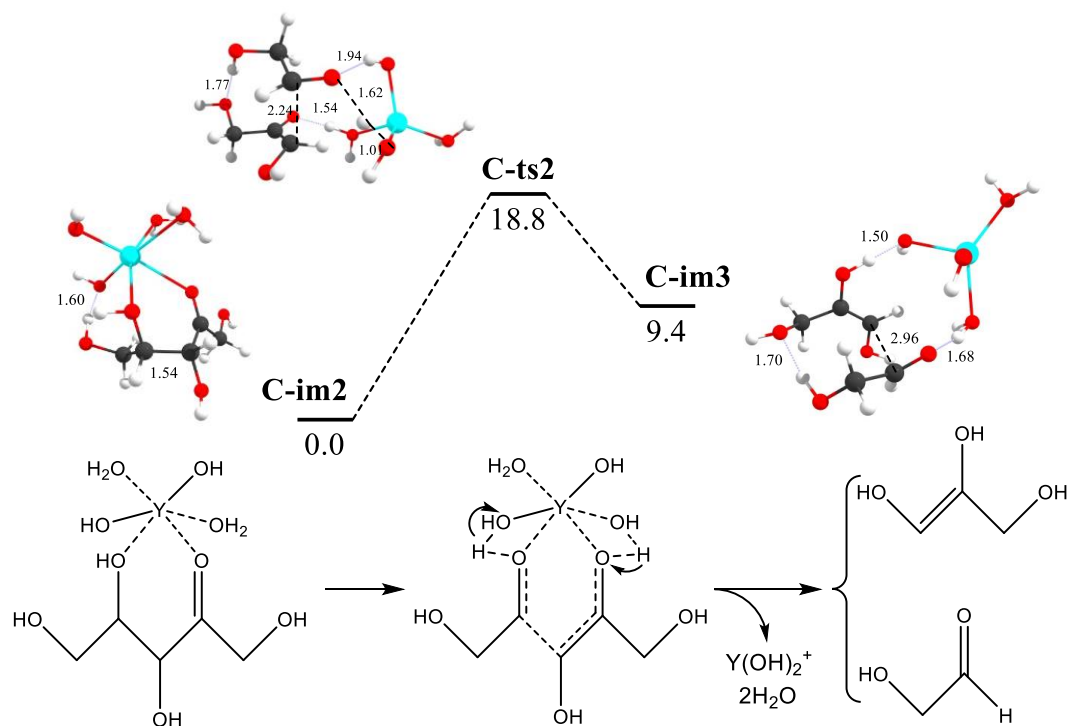
Figure S27. Energy profiles (in kcal mol^{-1}) and optimized structures (in Å) for the reaction pathway of xylulose conversion in the presence of Y(Ⅲ), Related to Figure 3.
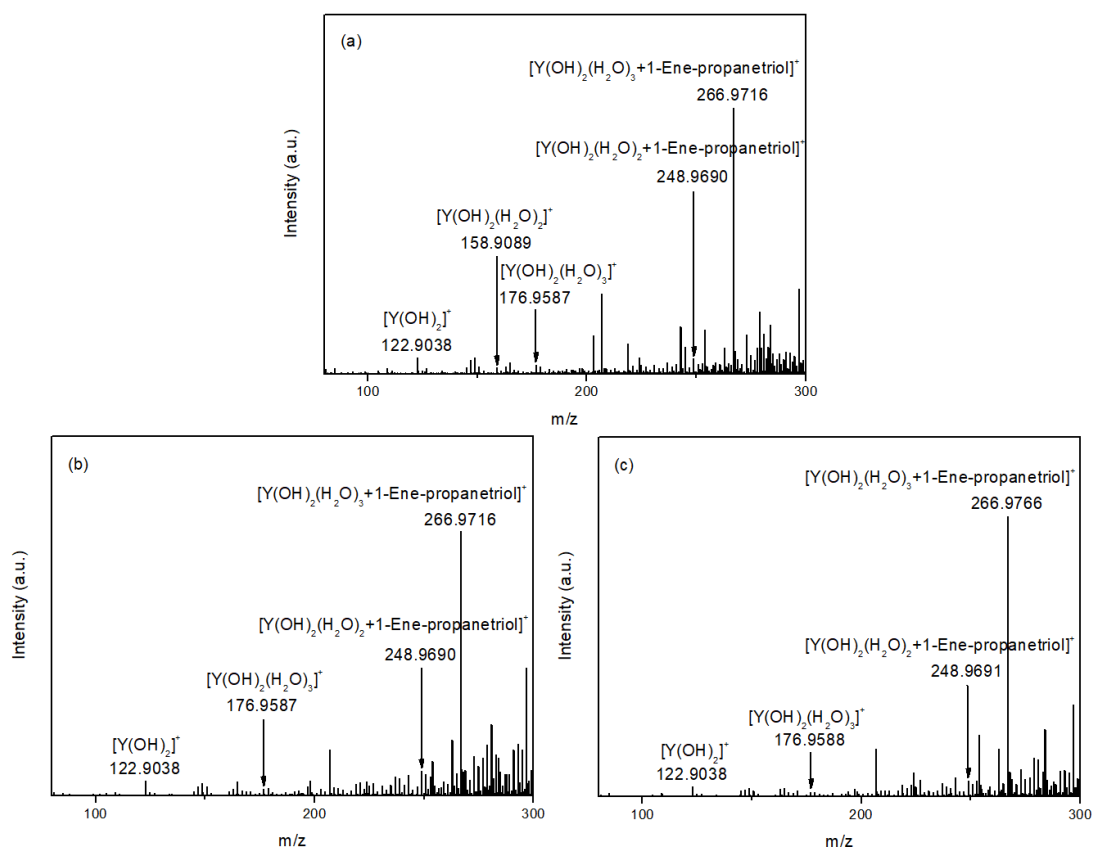
Figure S28. ESI-MS spectra of the liquid mixture derived from (a) DHA, (b) GLA, (c) PRA conversion in the presence of diluted Y(Ⅲ) in water after reaction. Reaction conditions: 0.12 g (26.7 mM) trioses; 50 mL H_2O; 6.6 mM YCl_3; 423 K, Related to Figure 3.
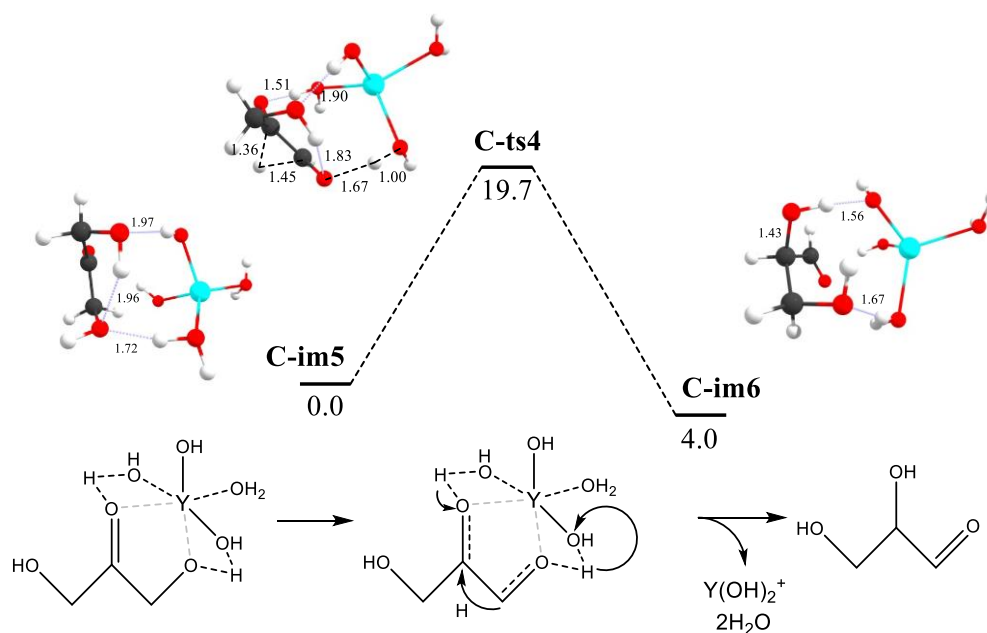
Figure S29. Energy profiles (in kcal mol^{-1}) and optimized structures (in Å) for the reaction pathway of the isomerization of DHA to GLA in the presence of Y(Ⅲ). As for the aldehyde-ketone isomerization of DHA to GLA, three times of hydrogen migration simultaneously happened: (i) the hydrogen atom of C1-OH was seized by the OH of $[Y(OH)_2(H_2O)_2]^+$; (ii) a hydrogen atom shifted from H_2O in $[Y(OH)_2(H_2O)_2]^+$ to C2=O; (iii) C1-H shifted to C2 in DHA, finally resulting in the formation of GLA, Related to Figure 3.
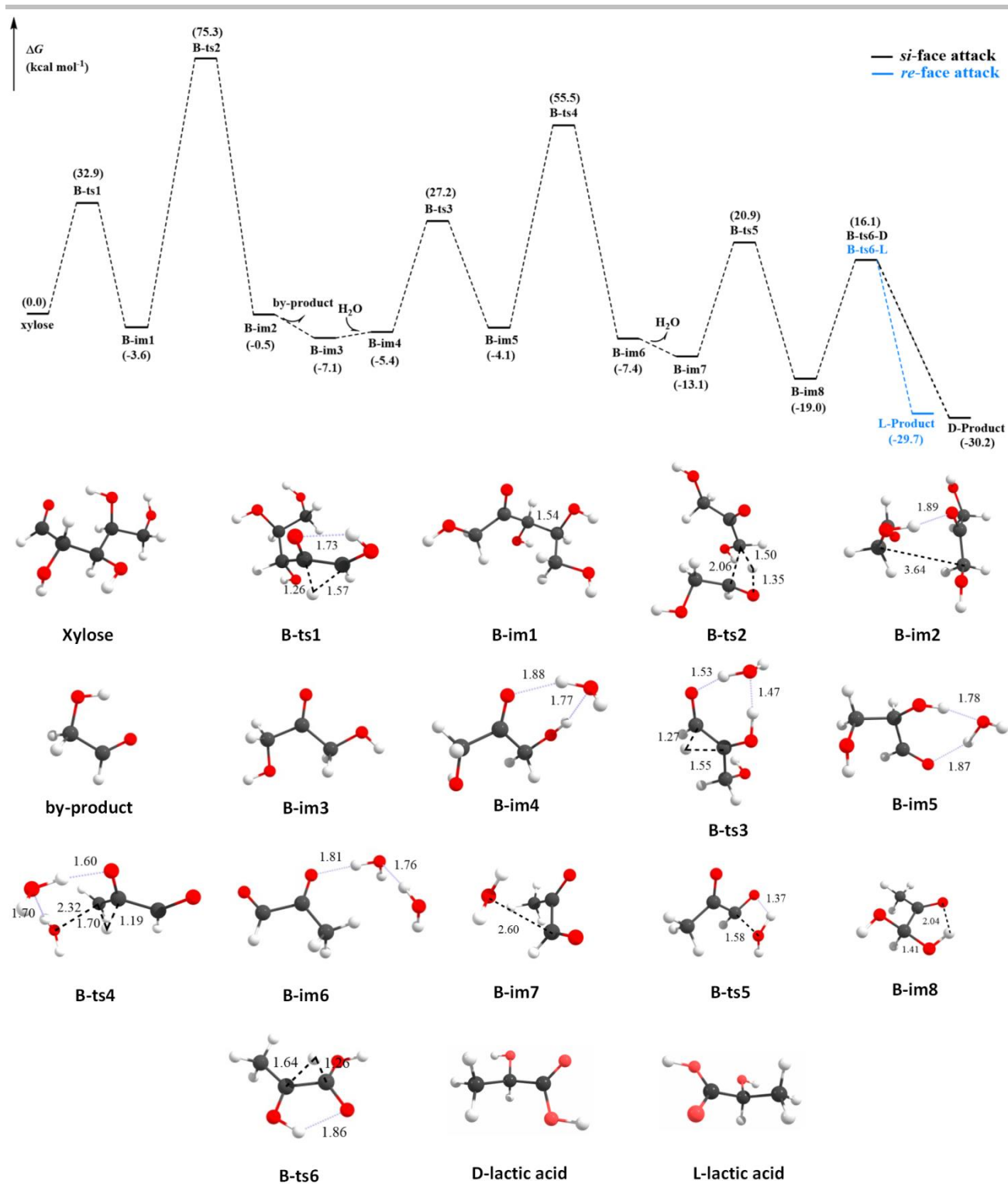
Figure S30. Calculated relative Gibbs energy (kcal mol⁻¹) profiles and the optimized structures (in Å) of species for the conversion of xylose to lactic acid in water via the cleavage of C3-C4 bond without catalyst (pathway 1), Related to Figure 3.
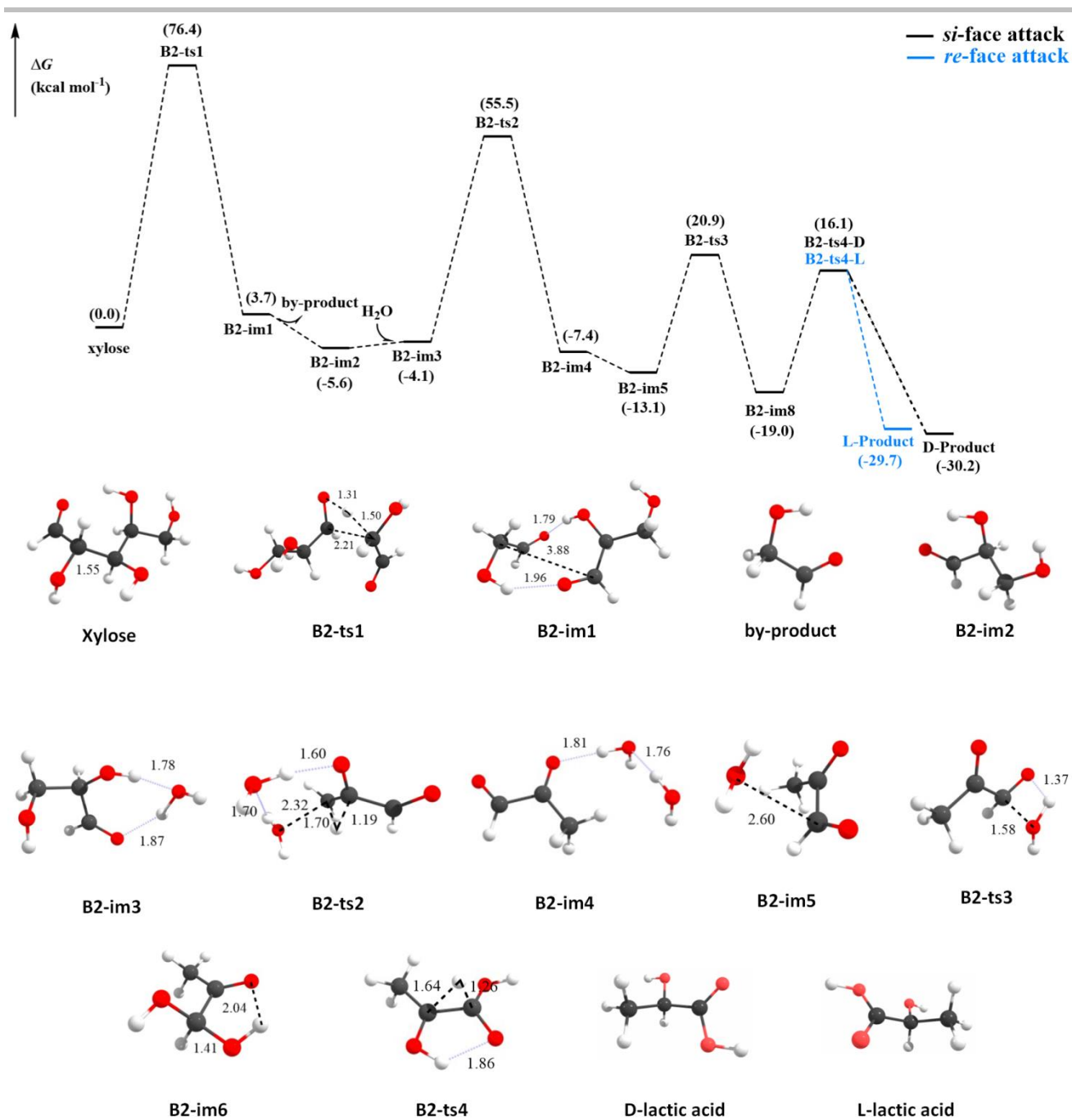
Figure S31. Calculated relative Gibbs energy profiles (in kcal mol⁻¹) and optimized structures (in Å) of species for the conversion of xylose to lactic acid via the cleavage of C2-C3 bond without catalyst (pathway 2), Related to Figure 3.
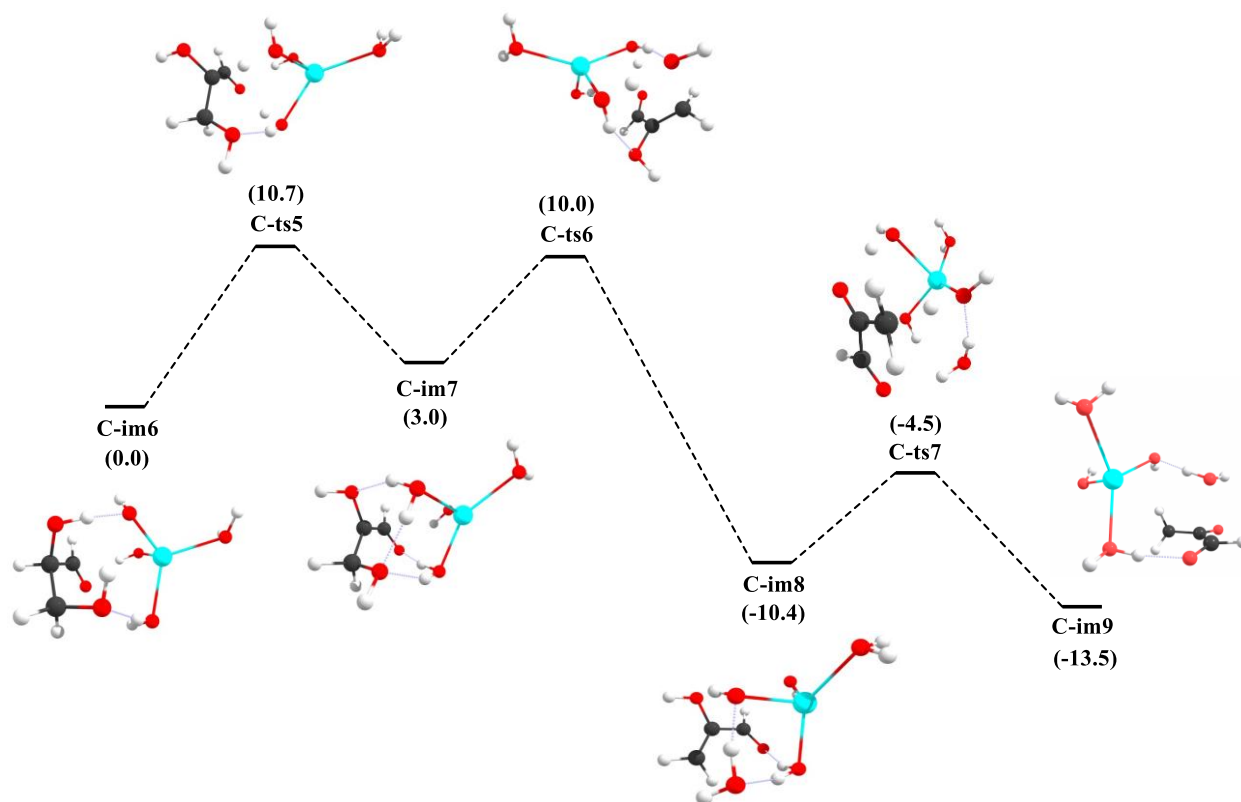
Figure S32. Energy profiles (in kcal mol^{-1}) and optimized structures (in Å) for the reaction pathway of GLA to PRA via the stepwise dehydration catalyzed by Y(Ⅲ) species, Related to Figure 3.

C-im9-D

C-im9-L

C-ts8-D

C-ts8-L

C-im10-D

C-im10-L

C-ts9-D2

C-ts9-L2

C-im11-D

C-im11-L

C-im11-D2

C-im11-L2

D-lactic acid

L-lactic acid
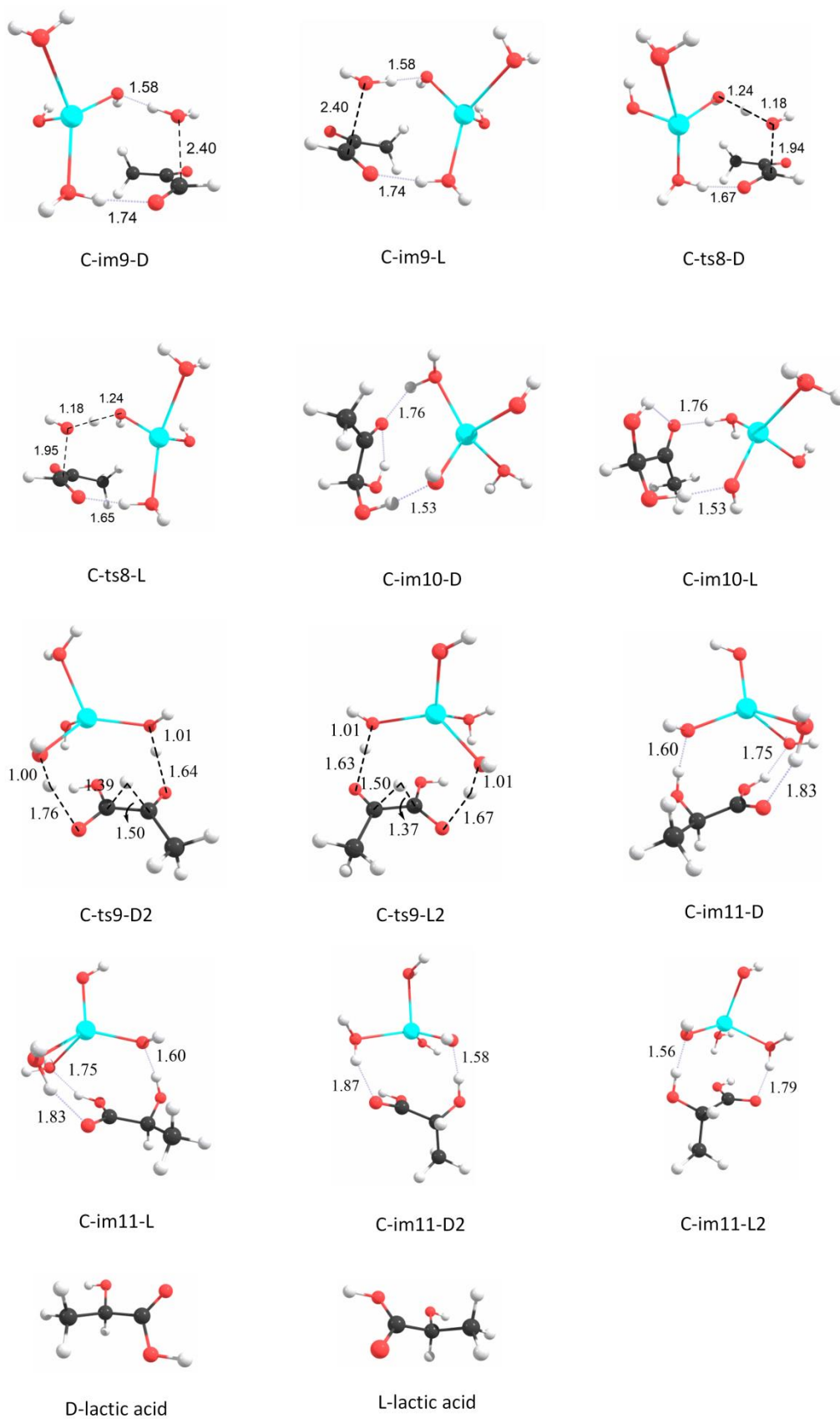
Figure S33. The optimized structures (in Å) of species involved in the conversion of PRA to D-/L-LaA for the calculated relative Gibbs energy profiles (in kcal mol^{-1}) in Fig. 4a, Related to Figure 3.
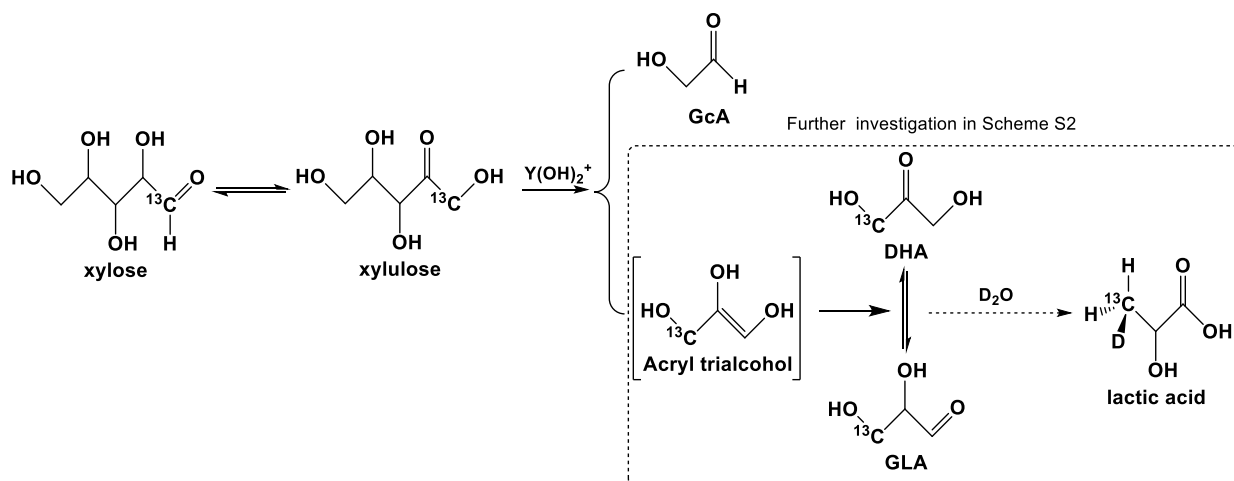
Scheme S1. Possible reaction pathway for the conversion of ^{13}C labeled xylose to DHA in the presence of $[Y(OH)_2(H_2O)_2]^+$ species in water. GcA represents glycolic aldehyde, Related to Figure 1, Figure 2 and Figure 3.
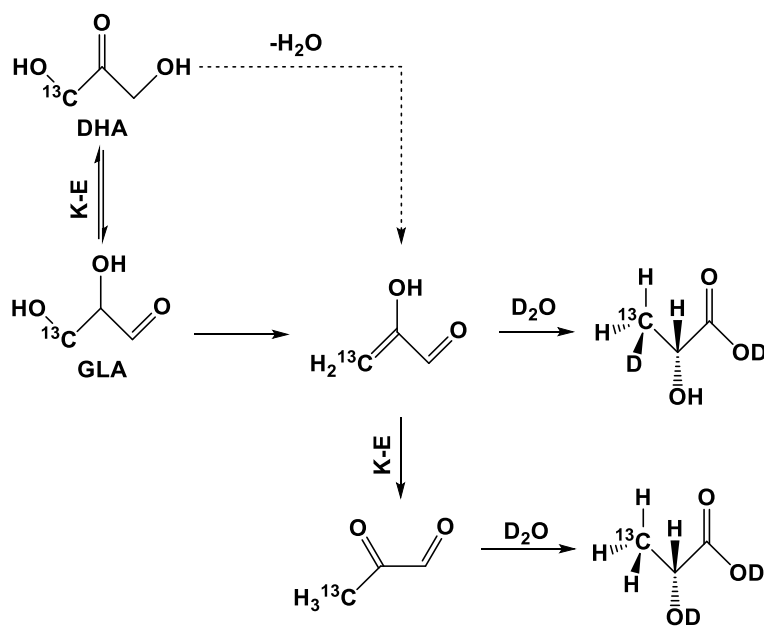
Scheme S2. Possible reaction pathway for the conversion of ^{13}C labeled trioses to deuterium lactic acid in the presence of Y(III) in D_2O. K-E represents keto-enol, Related to Figure 1, Figure 2 and Figure 3.

Table S1. The comparison to the literatures in catalytic synthesis of lactic acid, Related to Table 1.

Reactant	Xylose	Cellulose	Glucose	Glucose	Glucose	Fructose	Glucose
Catalyst	ZrO_2	Ni(II)	Co(II)	Pb(II)	Al(III)	Zn(II)	Sn-Beta
Yield/%	42[a]	6.4[b]	8.9[b]	71[b]	18[b]	24[b]	79.9[b]
Tem[c].	493 K	573 K	573 K	463 K	413 K	573 K	483 K
Time	40min	120 s	120 s	2 h	6 h	10 min	2 h
TOF/h^{-1}	0.26	2.2	3.0	2.6	0.6	6.4	-
D/L	---[d]	---[d]	---[d]	---[d]	---[d]	---[d]	---[d]
Ref.	Yang et al., 2015	Kong et al., 2008	Kong et al., 2008	Wang et al., 2013	Rasrendra et al., 2010	Bicker et al., 2005	Zan et al., 2018

[a] Molar yield of lactic acid; [b] Molar carbon yield; [c] reaction temperature; [d] Not found.

Table S2. The recyclability of Y(Ⅲ)[a], Related to Table 1.

Reuse times	1	2	3
Yield of total lactic acid (%)	85.6	86.7	86.1

[a] Reaction conditions: 0.20 g (26.7 mM) xylose; the mixture of 0.165 mmol recovered Y_2O_3 and 0.99 mmol HCl; 50 mL H_2O; N_2, 2 MPa; reaction time, 0.5 h; temperature, 493 K.

Table S3. The influence of HCl on the conversion of xylose to lactic acid[a], Related to Table 1.

Entry	Catalyst	Conversion of xylose (%)	Yield of lactic acid (%)
1	YCl_3[b]	99.8	87.3
2	HCl[c]	95.3	2.2
3	YCl_3 and HCl[d]	99.6	15.2

[a] Reaction conditions: 0.20 g (26.7 mM) xylose; 50 mL H_2O; N_2, 2 MPa; reaction time, 0.5 h; temperature, 493 K. [b] 6.6 mM YCl_3. [c] 40 mM HCl. [d] 6.6 mM YCl_3 and 40 mM HCl.

Table S4. The influence of YCl_3 on the conversion of trioses to lactic acid[a], Related to Figure 3.

Entry	Catalyst	Substrate	Conversion (%)	Yield of lactic acid (%)
1	YCl_3	Dihydroxyacetone	100	92.7
2	YCl_3	Glyceraldehyde	100	91.1
3	YCl_3	Pyruvaldehyde	100	93.0
4	---	Dihydroxyacetone	100	8.1
5	---	Glyceraldehyde	100	8.9
6	---	Pyruvaldehyde	100	12.0

[a] Reaction conditions: 0.12 g (26.7 mM) trioses; 50 mL H_2O; 6.6 mM YCl_3; N_2, 2 MPa; reaction time, 0.5 h; temperature, 493 K.

Table S5. Catalytic activities of Y(Ⅲ) for the formation of lactic acid from xylose in D_2O^a, Related to Figure 1 and Figure 2.

xylose (trioses) $\xrightarrow{D_2O}$ → $\xrightarrow{YCl_3}$ 2-hydroxy, 1-COOH, 3-CH_2D (HO–C2, O=C1–OH, $^3CH_2D$)

and → 2-hydroxy, 1-COOH, 3 (HO–C2, O=C1–OH)
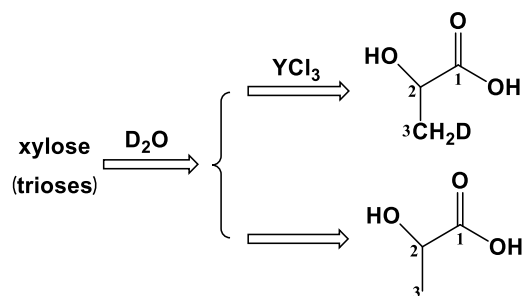
Entry	Substrate	Catalyst	Conversion (%)	Selectivity(%)	D content (%) C2	D content (%) C3
1	Xylose	---	91	3.0	Little[b]	---[c]
2	Xylose	YCl_3	99.8	78.4	---[c]	20
3	Lactic acid	---	13.3	---	---[c]	---[c]
4	Lactic acid	YCl_3	9.3	---	---[c]	---[c]
5	Dihydroxyacetone	YCl_3	100	92.7	---[c]	29
6	Glyceraldehyde	YCl_3	100	91.1	---[c]	26
7	Pyruvaldehyde	YCl_3	100	93.0	---[c]	---[c]
8	Dihydroxyacetone	---	100	8.1	---[c]	---[c]
9	Glyceraldehyde	---	100	8.9	---[c]	---[c]
10	Pyruvaldehyde	---	100	12.0	---[c]	---[c]

[a] Reaction conditions: 0.20 g (26.7 mM) xylose or 0.12 g (26.7 mM) trioses or lactic acid; 50 mL D_2O; 6.6 mM YCl_3; N_2, 2 MPa; reaction time, 0.5 h; temperature, 493 K. [b] Not detectable. [c] Below detection limit.

Table S6. Activation Gibbs energy barrier and Gibbs free energy values, Related to Figure 3.

Reaction step	Catalytic pathway[a] (kcal mol^{-1}) Catalyzed by $[Y(OH)_2(H_2O)_2]^+$	Non-catalytic pathway (kcal mol^{-1}) Pathway 1[b]	Non-catalytic pathway (kcal mol^{-1}) Pathway 2[c]
2→3	$\Delta G^{\neq}$=17.4; ΔG_r=-4.1	$\Delta G^{\neq}$=32.9; ΔG_r=-3.6	
3→4+5	$\Delta G^{\neq}$=18.8; ΔG_r=9.4	$\Delta G^{\neq}$=78.9; ΔG_r=3.1 (**3→7**)	$\Delta G^{\neq}$=76.4; ΔG_r=3.7 (**2→8**)
4→7	$\Delta G^{\neq}$=11.3; ΔG_r=-3.7		
7→8	$\Delta G^{\neq}$=19.7; ΔG_r=4.0	$\Delta G^{\neq}$=32.6; ΔG_r=1.3	
8→9	See in Table S7	$\Delta G^{\neq}$=59.6; ΔG_r=-3.3	$\Delta G^{\neq}$=59.6; ΔG_r=-3.3
9→11	See in Fig. 4a	$\Delta G^{\neq}$=34.0; ΔG_r=-5.9	$\Delta G^{\neq}$=34.0; ΔG_r=-5.9
11→12		$\Delta G^{\neq}$=35.1; ΔG_r=-10.7	$\Delta G^{\neq}$=35.1; ΔG_r=-10.7

$\Delta G^{\neq}$ and ΔG_r present Activation Gibbs energy barrier and Gibbs free energy values, respectively.
[a]The pathway was shown in Fig. 4a. [b]The pathway was shown in Fig. S30. [c]The pathway was shown in Fig. S31.

Table S7. Activation energy barrier and Gibbs free energy values for the GLA to PRA, Related to Figure 3.

Reaction step[a]	Activation energy barrier and Gibbs free energy values (kcal mol^{-1})	
	Direct dehydration	Stepwise dehydration
C-im6→C-im7		$\Delta G^{\neq}$=10.7; ΔG_r=3.0
C-im7→C-im8	$\Delta G^{\neq}$=34.8; ΔG_r=-13.5	$\Delta G^{\neq}$=7.0; ΔG_r=-13.4
C-im8→C-im9		$\Delta G^{\neq}$=5.9; ΔG_r=-3.1

[a]The detailed procedures and their code names are shown in Fig. 3.

$\Delta G^{\neq}$ and ΔG_r present Activation energy barrier and Gibbs free energy values, respectively.

Table S8. Cartesian coordinates for the catalytic and non-catalytic reaction of xylose to D-lactic acid/L-lactic acid, Related to Figure 3 and Figure 4.

The Related contents are showed in supplemental spreadsheet file.

Table S9. Effect of NaOH on the conversion of trioses to lactic acid[a], Related to Figure 3 and Figure 4.

Reactant	DHA	GLA	PRA
Yield of total lactic acid (%)	11.0	7.7	40.9

[a] Reaction conditions: 0.12 g (26.7 mM) trioses; 6.6 mM NaOH; N_2, 2 MPa; reaction time, 0.5 h; temperature, 493 K.

Table S10. TOF values in different catalytic cycles, Related to Figure 4.

Catalytic cycle	1	2	3	4	5	6	7	8	9	10
TOF/h^{-1}	1.49	8.02×10^{-1}	1.05×10^{-3}	3.75×10^{-3}	2.56	5.94×10^{-13}	1.84×10^{-4}	6.72×10^{-5}	2.37×10^{-7}	4.81×10^{-6}

1. Experienced transition state: C-ts1, C-ts2, C-ts3, C-ts4, C-ts5, C-ts6, C-ts7, C-ts8-D, C-ts9-D, from xylose to D-lactic acid; 2. Experienced transition state: C-ts1, C-ts2, C-ts3, C-ts4, C-ts5, C-ts6, C-ts7, C-ts8-L, C-ts9-L, from xylose to L-lactic acid; 3. Experienced transition state: C-ts1, C-ts2, C-ts3, C-ts4, C-ts5, C-ts6, C-ts7, C-ts8-L, C-ts9-D2, from xylose to D-lactic acid; 4. Experienced transition state: C-ts1, C-ts2, C-ts3, C-ts4, C-ts5, C-ts6, C-ts7, C-ts8-D, C-ts9-L2, from xylose to L-lactic acid; 5. Experienced transition state: C-ts1, C-ts2, C-ts3, C-ts4, C-ts5, C-ts6, C-ts7, from xylose to PRA; 6. Experienced transition state: C-ts1, C-ts2, C-ts3, C-ts4, C-ts5', from xylose to PRA; 7. Experienced transition state: C-ts8-D, C-ts9-D, from PRA to D-lactic acid; 8. Experienced transition state: C-ts8-L, C-ts9-L, from PRA to L-lactic acid; 9. Experienced transition state: C-ts8-L, C-ts9-D2, from PRA to D-lactic acid. 10. Experienced transition state: C-ts8-D, C-ts9-L2, from PRA to L-lactic acid;

Table S11. Results of Activation Strain Analysis (ASM) for two key chirality-controlling steps in the formation of lactic acid enantiomers (in kcal mol^{-1}), Related to Figure 4.

Transition state	$\Delta E^{\neq}$	$\Delta E^{\neq}_{strain}$			$\Delta E^{\neq}_{int}$
		Reactant	Catalyst	Sum	
C-ts9-D	7.9	93.8	3.2	97.0	-89.1
C-ts9-L	9.2	105.1	2.4	107.5	-98.3

Transparent Methods

Materials

Yttrium (III) chloride hexahydrate (99.99%), $CrCl_3 \cdot 6H_2O$ (99%), $AlCl_3 \cdot 6H_2O$ (99%), $Pb(NO_3)_2$ (99%) and ZrO_2 (99.9%) were obtained from Adamas-beta (Shanghai, China). $SnCl_2$ (99.99%) was purchased from Sigma-Aldrich. D-xylose (99%), dihydroxyacetone (98%), D_2O (99.8%), pyruvaldehyde (40 wt%), xylose (99%), xylan (95%, from corn core) and Microcrystalline cellulose (<80 mesh) were purchased from J&K Chemicals (Beijing, China). D-lactic acid (95%) and L-lactic acid (98%) were obtained from Alfa Aesar. Glyceraldehyde (93%) was purchased from APOLLO Scientific Limited. ^{13}C-C1 labeled D-xylose (99%) was purchased from Cambridge Isotope Laboratories (CIL), Inc. Corn straw was obtained from Fushun in Liaoning province of China and the size of corn straw powder ranged from 60–100 mesh. The corn straw powder was dried in an oven at 100 ℃ overnight before use. The ultrapure water of 18.25 $M\Omega \cdot cm^{-1}$ (298 K) was used after degasification. Other general reagents used in this work were purchased from J&K Chemicals (Beijing, China).

Catalytic reaction

The conversion of xylose, xylan, trioses, M-cellulose and corn straw were performed in a batch Parr autoclave. For a typical catalytic reaction of xylose, 0.20 g (1.33 mmol) xylose, 0.10 g (0.33 mmol) YCl_3, and 50 mL of water were added into the Parr autoclave. After the introduction of N_2 at a pressure of 2 MPa, the reactor was heated to the designed temperature (usually 493 K) with a stirring rate of 400 rpm for a certain time (usually 0.5 h). After reaction, the reactor was quenched with ice water mixture. The liquid products were subjected to the subsequent analysis. Each reaction was conducted for three times, and the resulted sample was tested for three times. The error was less than 3%.

Analytical methods of lactic acid

Qualitative and quantitative analysis of LaA enantiomers were performed on a Shimadzu LC-20AR HPLC, equipped with a variable wavelength detector (Model SPD-20A) and a CRS10W column (50 mm × 4.6 mm, a typical chiral column used to separate LaA enantiomers). The eluent was dilute $CuSO_4$ (1 mM) aqueous solution with a flow rate of 0.30 mL•min^{-1}, and the column temperature was kept at 308 K. The HPLC analysis of the mixture of D- and L-LaA was shown in Fig. S1. The concentrations of D-LaA and L-LaA were determined by comparison to the standard calibration curves. Other liquid products were analyzed by DIONEX U3000 HPLC, equipped with a variable wavelength detector (Model VWD-3x00(RS)) and a refractive index detector (Model RI-101, Shodex) as well as a HPX-87H column (300 mm × 7.8 mm, Bio-Rad). The eluent was dilute H_2SO_4 aqueous solution (5 mM) with a flow rate of 0.60 mL•min^{-1}, and the column temperature was maintained at 323 K. The concentrations of all components were determined by comparison to the standard calibration curves.

In general, the relevant literature for the synthesis of lactic acid from xylose (Yang et al., 2015; Yang et al., 2016) calculates lactic acid yield on the assumption that per mole of xylose can yield only one mole of lactic acid, while it is assumed that two moles of lactic acid can be formed from one mole of glucose (Wang el al., 2013; Deng et al., 2018). According to these literatures, the yield of lactic acid in our work is calculated using the same definition, which is listed as follows:

When C5 sugar is used, the molar yield of LaA is calculated by:

Y%=((moles of obtained D-LaA + moles of obtained L-LaA))/(moles of xylose in feedstock) × 100

When C6 sugar is used, the molar yield of LaA is calculated by:

Y%=((moles of obtained D-LaA + moles of obtained L-LaA))/(2×moles of glucose in feedstock) × 100

Particularly, the yield of lactic acid from corn stalk is calculated based on the converted cellulose and

hemicellulose, and thus, the yield of LaA from corn stalk is defined by the following equations:

Molar yield of LaA: Y%=((moles of obtained D-LaA + moles of obtained L-LaA))/(moles of xylose in feedstock + 2× moles of glucose in feedsock)×100.

Quantitative method of other products:

The conversion of reactant (X), yield (Y) of by-products, as well as the carbon balance, are defined by the following equations:

$$X\% = \frac{\text{moles of initial reactant} - \text{moles of final reactant}}{\text{moles of initial reactant}} \times 100 \tag{1}$$

$$\text{Molar yield of formic acid: } Y\% = \frac{\text{moles of formic aicd}}{5 \times \text{moles of initial reactant}} \times 100 \tag{2}$$

$$\text{Molar yield of glycolic acid: } Y\% = \frac{\text{moles of glycolic acid}}{2 \times \text{moles of initial reactant}} \times 100 \tag{3}$$

$$\text{Molar yield of other products: } Y\% = \frac{\text{moles of other products}}{\text{moles of initial reactant}} \times 100 \tag{4}$$

$$\text{carbon balance}\% = \frac{\text{output of carbon in mole (including lactci acid and the detected byproducts)}}{\text{input of carbon in mole (feedstock)}} \times 100 \tag{5}$$

$$\text{Selectivity: } S\% = \frac{\text{moles of products}}{\text{moles of initial reactant} - \text{moles of final reactant}} \times 100 \tag{6}$$

ESI-MS/MS.

Electron spin ionization-mass spectroscopy/mass spectroscopy (ESI-MS/MS) was collected in continuum mode. A Micromass Quattro Micro mass spectrometer (Waters) was used with the following operating parameters: capillary voltage, 2.8 kV; extractor voltage, 5 V; sample cone voltage, 20 V; source temperature, 363 K; desolvation temperature, 423 K; cone gas (N_2) flow, 40 L•h^{-1}. A collision energy of 20 eV was used for the collision-induced dissociation stage in the MS/MS measurements. The data acquisition and analyses were performed using Masslynx v 4.1 software (Waters).

NMR Spectrometry.

NMR spectra were obtained using an Advance II 400 MHz NMR spectrometer (Bruker). ^{1}H NMR spectra were measured at 400.13 MHz (pulse width, 9.75 μs; acquisition time, 4.0894 μs; 16 scans; 298 ± 1 K; D_2O for field lock; TSP in capillary as external standard for 1H δ 0.00). ^{13}C NMR spectra were measured at 100.62 MHz (pulse width, 9.80 μs; acquisition time, 1.3631 μs; 256 scans; 298 ± 1 K; D_2O for field lock; TSP in capillary as external standard for ^{13}C δ 0.00).

Computational details.

All calculations in this work were performed using Gaussian 09 program package (Frisch et al., 2013). Geometries were fully optimized in water solvent at the B3LYP/def2SVP level (Weigend et al., 2005) and characterized by frequency analysis at 298 K. The self-consistent reaction field (SCRF) method based on the universal solvation model SMD (Marinich et al., 2009) was adopted to evaluate the effect of solvent. Dispersion corrections were computed with Grimme's D3(BJ) method in optimization (Grimme et al., 2010). The intrinsic reaction coordinate (IRC) path was traced to check the energy profiles connecting each transition state to two associated minima of the proposed mechanism (Gonzalez et al., 1989). Unless specified, the Gibbs free energies corrected by both solvation and zero-point vibrational effects at the B3LYP-D3(BJ)/def2TZVP(SMD, water) level at 298 K were used in the discussion. In addition to 298 K, thermal corrections were also assessed at 493 K to explore the temperature effect on Gibbs free energy, and results showed that the temperature effect was not remarkable in this work. To understand the factors

affecting the chirality, we performed Activation Strain Analysis (ASM) (Wolters and Bickelhaupt, 2015; Zeist and Bickelhaupt, 2010; Fernandez, 2014). (or distortion/strain model calculation) by decomposing activation barrier into the distortion energy (E_{strain}) and the interaction energy (E_{int}).

The efficiency of the catalyst can be determined by the turnover frequency (TOF) of the catalytic cycle. Based on the transition state theory (TST), the TOF can be calculated by Eqs. (i) and (ii) proposed by Kozuch et al. (Kozuch and Shaik, 2006; Kozuch and Shaik, 2008), in which δE (the energetic span (Koo et al., 2010; Kozuch et al., 2015; Amatore and Jutand, 1999)) is defined as the energy difference between the summit and trough of the catalytic cycle.

$$\text{TOF} = \frac{k_B T}{h} e^{-\frac{\delta E}{RT}}$$

(i)

$$\delta E = \begin{pmatrix} G_{TDTS} - G_{TDI} & \text{if TDTS appears after TDI} \\ G_{TDTS} - G_{TDI} + \Delta G_r & \text{if TDTS appears before TDI} \end{pmatrix}$$

(ii)

where k_B is the Boltzmann constant, T is the absolute temperature, and h is the Planck constant. G_{TDTS} and G_{TDI} are the Gibbs free energies of the TOF determining transition state (TDTS) and the TOF determining intermediate (TDI), and ΔG_r is the global free energy of the whole cycle.

Supplemental Text

Note S1. Recovery of yttrium ion.

We used the classical chemical precipitation method (Desouky et al., 2009) to recover yttrium ion from reaction solution in the form of yttrium oxalate precipitate, and oxalic acid (1 M) was employed as the precipitant. After calcination in muffle furnace at 1073 K for 2 h, solid Y_2O_3 was obtained. The obtained Y_2O_3 was further acidified by HCl, YCl_3 could be obtained again, which could be used for the next run. The typical operation processes were listed as follows:

(1) The concentration of yttrium ion in the reaction solution was determined by chemical titration, and EDTA (0.01 M) was employed as the titrant with xylenol orange as the indicator (Zhang et al., 2014; Li et al., 2007).

(2) Stoichiometric oxalic acid was added into the reaction solution (20 mL), and the system was agitated for ten minutes to make the reaction complete. Then, the mixture was centrifuged for five minutes at a rotation rate of 2000 rpm.

(3) The precipitate was collected, and then calcined at 1073 K for 2 h in a muffle furnace. The precipitated yttrium (III) could be calculated based on the mass balance after determination the concentration of the remaining yttrium ion in the supernatant. The results showed that more than 92% of yttrium ion was transformed into yttrium oxalate precipitate.

(4) After calcination, Y_2O_3 was obtained. The recycled Y_2O_3 showed very similar XRD spectra (Figure S5) with the commercial Y_2O_3, proving the high purity of recycled Y_2O_3. The recycled Y_2O_3 could be dissolved with stoichiometric HCl for the next catalytic reaction. After recycled three times, the catalytic activity had no obvious reduction (Table S2).

Note S2. Calculation of corrected ΔG of the hydrolysis of Y(III) to $[Y(OH)_2(H_2O)_2]^+$ species.

Hydrolysis equation: $$YCl_3 \cdot 6H_2O \leftrightharpoons Y(OH)_2(H_2O)_2{}^+ + 3Cl^- + 2H_3O^+$$

$$\Delta G_r^0 = \sum G_{r(products)}^0 - \sum G_{r(reactants)}^0$$

(1)

Because the Y(III) species for hydrolysis are minority, the concentration of all the components should be taken for considerations (Ren et al., 2016). Therefore, the G_r^0 should be corrected by the following

equations (Bernales et al., 2012):

$$G_r = G_r^0 + RT\ln\frac{C}{C_0} \tag{2}$$

Where R is the universal gas constant, T is the reaction temperature, C_0 is the standard molar concentration (1 mol·L^{-1}), G_r is the corrected (practical) Gibbs free energy and G_r^0 is denoted as the standard Gibbs energy. The practical molar concentration ([YCl_3·$6H_2O$]=6.6 mmol·L^{-1}; [H_2O]=55.6 mol·L^{-1}; [H_3O^+]=$10^{-5.48}$ mol·L^{-1}; [Cl^-]=19.8 mmol·L^{-1}; [$Y(OH)_2(H_2O)_2^+$]=$6.6\times10^{-9.06}$ mol·L^{-1}, which is calculated based on the results of Liu et al. (Liu et al., 2012)) of species can be obtained, respectively, under our mentioned reaction conditions. Therefore, the practical ΔG_r should be calculated by the corrected equation:

$$\Delta G_r = \sum G_{r(products)} - \sum G_{r(rectants)} \tag{3}$$

According to the equation (1), (2) and (3), the final practical ΔG_r was calculated as -26.9 kcal mol^{-1}, that is, the stabilization energy of Y(III) hydrolyzing to [$Y(OH)_2(H_2O)_2$]$^+$ species was 26.9 kcal mol^{-1}.

Supplemental References

Yang, L., Su, J., Carl, S., Lynam, J. G., Yang, X., Lin, H. (2015). Catalytic conversion of hemicellulosic biomass to lactic acid in pH neutral aqueous phase media. Appl. Catal. B: Environ. *162*, 149-157.

Kong, L., Li, G., Hua, W., He, W., Fang, L. (2008). Hydrothermal catalytic conversion of biomass for lactic acid production. J. Chem. Technol. Biotechnol. *83*, 383-388.

Wang, Y., Deng, W., Wang, B., Zhang, Q., Wan, X., Tang, Z., Wang, Y., Zhu, C., Cao, Z., Wang, G., Wan, H. (2013). Chemical synthesis of lactic acid from cellulose catalysed by lead(II) ions in water. Nat. Commun. *4*, 2141.

Rasrendra, C. B., Makertihartha, I. G. B. N., Adisasmito, S., Heeres, H. J., (2010). Green Chemicals from d-glucose: Systematic Studies on Catalytic Effects of Inorganic Salts on the Chemo-Selectivity and Yield in Aqueous Solutions. J. Top. Catal. 53, 1241-1247.

Bicker, M., Endres, S., Ott, L., Vogel, H. (2005). Catalytical conversion of carbohydrates in subcritical water: A new chemical process for lactic acid production. J. Mol. Catal. A *239*, 151-157.

Zan Y., Sun Y., Kong L., Miao G., Bao L., Wang H., Li S., Sun Y. (2018). Formic Acid-Induced Controlled-Release Hydrolysis of Microalgae (Scenedesmus) to Lactic Acid over Sn-Beta Catalyst. ChemSusChem *11*, 2492-2496.

M.J. Frisch, G.W. Trucks, H.B. Schlegel, G.E. Scuseria, M.A. Robb, J.R. Cheeseman, G. Scalmani, V. Barone, B. Mennucci, G.A. Petersson, H. Nakatsuji, M. Caricato, X. Li, H.P. Hratchian, A.F. Izmaylov, J. Bloino, G. Zheng, J.L. Sonnenberg, M. Hada, M. Ehara, K. Toyota, R. Fukuda, J. Hasegawa, M. Ishida, T. Nakajima, Y. Honda, O. Kitao, H. Nakai, T. Vreven, J.A. Montgomery, J.J.E. Peralta, F. Ogliaro, M. Bearpark, J.J. Heyd, E. Brothers, K.N. Kudin, V.N. Taroverov, T. Keith, R. Kobayashi, J. Normand, K. Raghavachari, A. Rendell, J.C. Burant, S.S. Iyengar, J. Tomasi, M. Cossi, N. Rega, J.M. Millam, M. Klene, J.E. Knox, J.B. Cross, V. Bakken, C. Adamo, J. Jaramillo, R. Gomperts, R.E. Stratmann, O. Yazyev, A. J. Austin, R. Cammi, C. Pomelli, J. W. Ochterski, R.L. Martin, K. Morokuma, V.G. Zakrzewski, G.A. Voth, P. Salvador, J.J. Dannenberg, S. Dapprich, A.D. Daniels, O. Farkas, J.B. Foresman, J.V. Ortiz, J. Cioslowski, D.J. Fox, (2013). Gaussian 09 (Revision D.01), I. Gaussian, Wallingford, CT.

Weigend, F., Ahlrichs, R. (2005). Balanced basis sets of split valence, triple zeta valence and quadruple zeta valence quality for H to Rn: Design and assessment of accuracy. Phys. Chem. Chem.Phys. *7*, 3297-3305.

Marenich, A. V., Cramer, C. J., Truhlar, D. G. (2009). Performance of SM6, SM8, and SMD on the SAMPL1 Test Set for the Prediction of Small-Molecule Solvation Free Energies. J. Phys. Chem. B **2009**, *113*, 4538-4543.

Grimme, S., Antony, J., Ehrlich, S., Krieg, H. (2010). A consistent and accurate ab initio parametrization of density functional dispersion correction (DFT-D) for the 94 elements H-Pu. J. Chem. Phys. *132*, 154104.

Gonzalez, C., Schlegel, H. B. (1989). An improved algorithm for reaction path following. J. Chem. Phys. *90*, 2154.

Wolters, L. P., Bickelhaupt, F. M. (2015). The activation strain model and molecular orbital theory. Chem. Soc. Rev. *5*, 4953-4967.

Zeist, W. J. V., Bickelhaupt, F. M. (2010). The activation strain model of chemical reactivity. Org. Biomol. Chem. *8*, 3118-3127.

Fernandez, I. (2014). Combined activation strain model and energy decomposition analysis methods: a new way to understand pericyclic reactions. Phys. Chem. Chem. Phys. *16*, 7662-7671.

Kozuch, S., Shaik, S. (2006). A combined kinetic-quantum mechanical model for assessment of catalytic cycles: application to cross-coupling and Heck reactions. J. Am. Chem. Soc. *128*, 3355-3365.

Kozuch, S., Shaik, S. (2008). Kinetic-Quantum Chemical Model for Catalytic Cycles: The Haber-Bosch Process and the Effect of Reagent Concentration. J. Phys. Chem. A *112*, 6032-6041.

Koo, H., Huh, M. S., Sun, I. C., Yuk, S. H., Choi, K., Kim, K., Kwon, I. C. (2011). In vivo targeted delivery of

nanoparticles for theranosis. Acc. Chem. Res. *44*, 1018-1028.

Kozuch, S. (2015). Steady State Kinetics of Any Catalytic Network: Graph Theory, the Energy Span Model, the Analogy between Catalysis and Electrical Circuits, and the Meaning of "Mechanism". ACS Catal. *5*, 5242-5255.

Amatore, C., Jutand, A. (1999). Mechanistic and Kinetic Studies of Palladium Catalytic Systems. J. Organomet. Chem. *576,* 254-278.

Desouky, O. A., Daher, A. M., Abdel-Monem, Y. K., Galhoum, A. A. (2009). Liquid-liquid extraction of yttrium using primene-JMT from acidic sulfate solutions. Hydrometallurgy *96*, 313-317.

Zhang, C., Wang, L., Huang, X., Dong, J., Long, Z., Zhang, Y. (2014). Yttrium extraction from chloride solution with a synergistic system of 2-ethylhexyl phosphonic acid mono-(2-ethylhexyl) ester and bis(2,4,4-trimethylpentyl) phosphinic acid. Hydrometallurgy 7, 147–148.

Li, W., Wang, X., Zhang, H., Meng, S., Li, D. (2007). Solvent extraction of lanthanides and yttrium from nitrate medium with CYANEX 925 in heptane. J. Chem. Technol. Biotechnol. *82*, 376-381.

Ren, L. K., Yang, H. Q., Hu, C. W. (2016). Theoretical Study on the Catalytic Oxidation Mechanism of 5-Hydroxymethylfurfural to 2, 5-Diformylfuran by PMo-Containing Keggin Heteropolyacid. Catal. Sci. Technol. *6*, 3776-3787.

Bernales, V. S., Marenich, A. V., Contreras, R., Cramer, C. J., Truhlar, D. G. (2012). Quantum Mechanical Continuum Solvation Models for Ionic Liquids. J. Phys. Chem. B *116*, 9122-9129.

Liu, X., Lu, X., Wang, R., Zhou, H. (2012). First-principles molecular dynamics study of stepwise hydrolysis reactions of Y^{3+} cations. Chem. Geol. *334*, 37-43.